WILEY-VCH

DOI: 10.1002/ ((please add manuscript number))
Article type: Full Paper

Engineered Multifunctional Albumin-Decorated Porous Silicon Nanoparticles for FcRn Translocation of Insulin

João P. Martins, Roberto D'Auria, Dongfei Liu, Flavia Fontana, Mónica P. A. Ferreira, Alexandra Correia, Marianna Kemell, Karina Moslova, Ermei Mäkilä, Jarno Salonen, Luca Casettari, Jouni Hirvonen, Bruno Sarmento, and Hélder A. Santos**

J. P. Martins, R. D'Auria, Dr. D. Liu, F. Fontana, M. P. A. Ferreira, A. Correia, E. Mäkilä, Prof. J. Hirvonen, Prof. H. A. Santos
Drug Research Program, Division of Pharmaceutical Chemistry and Technology, Faculty of Pharmacy, University of Helsinki, Helsinki FI-00014, Finland
E-mail: joao.martins@helsinki.fi; helder.santos@helsinki.fi

R. D'Auria, Prof. L Casettari
Department of Biomolecular Sciences, School of Pharmacy, University of Urbino, Urbino (PU) 61029, Italy

Dr. D. Liu, Prof. H. A. Santos
Helsinki Institute of Life Science (HiLIFE), University of Helsinki, Helsinki FI-00014, Finland

Karina Moslova, Dr. M. Kemell
Department of Chemistry, University of Helsinki, Helsinki FI-00014, Finland

E. Mäkilä, Prof. J. Salonen
Department of Physics and Astronomy, University of Turku, Turku FI-20014, Finland

Prof. B. Sarmento
i3S - Instituto de Investigação e Inovação em Saúde, University of Porto, 4200-135 Porto, Portugal

Prof. B. Sarmento
INEB - Instituto de Engenharia Biomédica, University of Porto, 4200-135 Porto, Portugal

Prof. B. Sarmento
CESPU - Instituto de Investigação e Formação Avançada em Ciências e Tecnologias da Saúde, 4585-116 Gandra, Portugal

Keywords: albumin; FcRn; insulin; nanoparticles; porous silicon

Abstract

The last decade has seen remarkable advances in the development of drug delivery systems as alternative to parenteral injection-based delivery of insulin. Neonatal Fc receptor (FcRn)-mediated transcytosis has been recently proposed as a strategy to increase the transport of drugs across the intestinal epithelium. FcRn-targeted nanoparticles (NPs) could hijack the FcRn transcytotic pathway, and cross the epithelial cell layer. In this study, a novel nanoparticulate system for insulin delivery based on porous silicon NPs is proposed. After surface conjugation with albumin and loading with insulin, the NPs are encapsulated into a pH-responsive polymeric particle by nanoprecipitation. The developed NP formulation shows controlled size and homogeneous size distribution. TEM images show successful encapsulation of the NPs into pH-sensitive polymeric particle. No insulin release is detected at acidic conditions, but a controlled release profile is observed at intestinal pH. Toxicity studies show high compatibility of the NPs with intestinal cells. *In vitro* insulin permeation across the intestinal epithelium showed a *ca.* 5-fold increase when insulin is loaded into FcRn-targeted NPs. Overall, these FcRn-targeted NPs offer a toolbox in the development of targeted therapies for oral delivery of insulin.

1. Introduction

Diabetes mellitus is the most prevalent metabolic disorder worldwide, being the fourth leading cause of death in developed countries.[1] Type 1 diabetes mellitus (T1DM) is commonly prevalent in children and adolescents, due to the lack of capability of the endocrine system to produce insulin, as a consequence of immune-mediated β-islet cells destruction.[2] Once diagnosed, the management of T1DM requires lifelong insulin treatment that, beyond the numerous disease-associated complications,[2] depends on frequent and painful injections. Therefore, there is high commercial interest in exploring alternative routes for insulin administration.

Oral delivery is the most widely used and preferred form of drug administration.[3] However, the efficiency of such therapeutic strategy depends on the successful delivery of drugs to the right cells/tissues. The entrapment of drugs into nanoparticles (NPs) has been gaining tremendous relevance in this field.[4, 5] NPs are already being developed under precise control of their size and shape to overcome low drug solubility, dissolution, and poor bioavailability. Additionally, NP encapsulation can protect drugs from enzymatic degradation and pH effects in the hostile gastrointestinal tract, and enhance their transmucosal transport,[6, 7] allowing for a temporally and spatially controlled and sustained release.[8] Moreover, NP surface can be modified with ligands to target specific cells/tissues, improving their ability to be retained at the site of action, further enhancing therapeutic efficiency and lowering off-target effects.[9-11] Over the years, we have been focused on the development of functionalized nanomedicines and their application in different pharmaceutical and biomedical fields, with particular attention to diabetes therapy.[12-14] However, despite the great advances achieved so far, the intestinal epithelium still represents an ultimate barrier for nanoencapsulated drugs, and their transport across the epithelial cell layer is yet to be achieved at optimum levels. Receptor-mediated transcytosis has been recently proposed as a potential strategy to overcome this limitation.[15]

Nanotechnology can profit from receptor-mediated transcytosis and potentiate bioavailability of orally delivered drugs, and here the neonatal Fc receptor (FcRn) seems to be the new player.[16] FcRn is a member of the major histocompatibility complex (MHC) class I molecules found on the surface of epithelial, endothelial and myeloid lineages.[16] In the intestinal microenvironment, FcRn works as a dual binding receptor transporting immunoglobulin G (IgG) and albumin across the polarized cell barrier, protecting them from intracellular catabolic degradation.[16] Once reaching a luminal pH of 6.0–6.5, substances containing the Fc portion of IgG or albumin favorably bind to FcRn at the apical surface of epithelial cells. They are then transcytosed by endosomes and released into the underlying extracellular space, where a physiological pH is found.[17] Hence, FcRn is able to create high affinity bonds in the acidic segments of the small intestine, where the majority of drug absorption occurs.[18, 19] For these reasons, decorating NPs with the albumin emerges as promising strategy to promote the transport of drugs across the intestinal epithelium. We hypothesize that NPs encapsulating insulin and functionalized with albumin could hijack the FcRn transport pathway, and cross the epithelial cell layer.

In the present study, a novel nanoparticulate system for efficient insulin delivery across intestinal cells was developed (**Scheme 1**). Due to the unprecedented advances shown in previous studies, porous silicon (PSi) NPs were used as nanocarrier.[20-22] After albumin conjugation and insulin loading, the particles were individually encapsulated into a pH-sensitive polymeric particle, in order to protect them from harsh gastrointestinal tract conditions. The developed formulation was tested for size, morphology, pH-responsiveness, and insulin release. *In vitro* cell viability and insulin permeability were also evaluated.

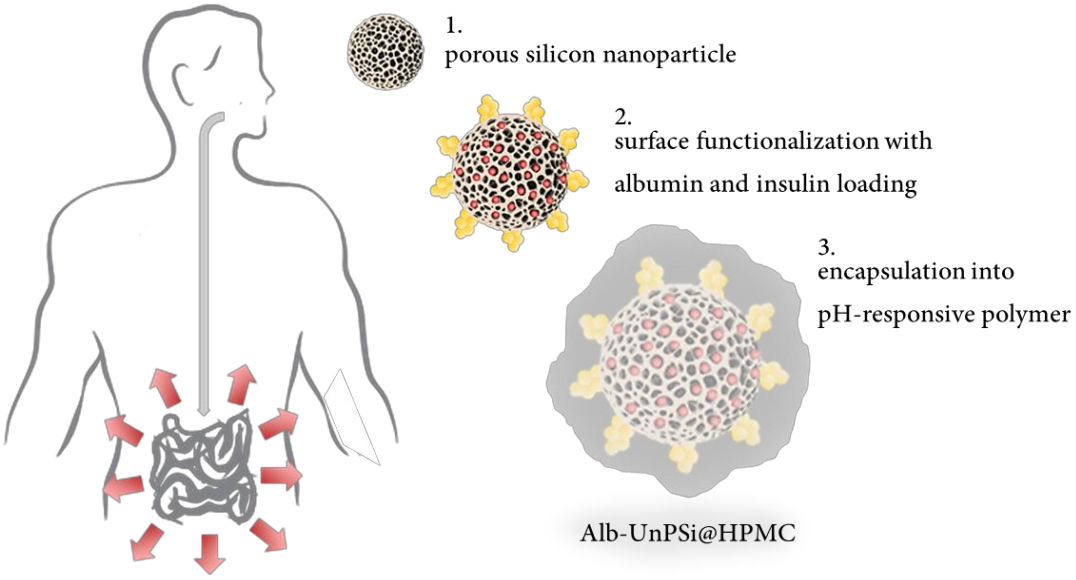

Scheme 1. Schematic representation of the engineered multifunctional nanoparticles developed in this study, consisting of insulin loaded albumin-functionalized PSi NPs encapsulated into HPMC (Alb-UnPSi@HPMC), for FcRn-targeted therapy of diabetes after oral administration. Image created using Servier Medical Art.

2. Results and discussion

2.1. Preparation and physicochemical characterization of the NPs

The core undecylenic acid modified thermally hydrocarbonized porous silicon (UnPSi) NPs were prepared by a top-down approach, using an electrochemical anodization method, followed by surface stabilization by thermal hydrocarbonization and modification by undecylenic acid treatment.[23, 24] Dynamic light scattering (DLS) analysis was performed to characterize the produced NPs in terms of size, polydispersion index (PdI), and surface charge. The bare NPs showed a particle size of 162 ± 3 nm (**Figure 1a**), with negative surface charge of –37 ± 1 mV (Figure 1b). To achieve an FcRn-targeted system, the surface of the NPs was further modified with albumin. A carbodiimide crosslinking using EDC/NHS reaction was employed to promote an amide bond between albumin and UnPSi NPs, forming Alb-UnPSi. The size of the resulting NPs increased (238 ± 6 nm; Figure 1a) when compared to the bare UnPSi, suggesting the successful functionalization of the surface of the NPs. Additionally, albumin in solution showed a surface charge of –12.00 ± 1.28 mV. Therefore, the increase in the surface charge of the NPs

to –12 mV (Figure 1b) further supported the successful surface functionalization of the NPs with albumin. In order to render the NPs with pH-responsive properties and protect insulin from the harsh stomach conditions, Alb-UnPSi NPs were encapsulated in hypromellose acetate succinate (H grade fine powders; HPMC) by nanoprecipitation. HPMC is an FDA approved polymer with pH-dependent solubility, which has been extensively used as enteric coating material.[7] It remains intact at acidic conditions, and becomes deprotonated and dissolved at pH ≥ 6.5. The encapsulation of the NPs in the polymer resulted in an increase on the size of the particles to 375 ± 30 nm. The negative charge of the ionized succinate groups in HPMC[25] provided the NPs with an expected negative surface charge of –33 mV. The PdI of bare and albumin decorated NPs was 0.10 ± 0.01 and 0.12 ± 0.02, respectively, while the final nanosystem showed an increase to 0.41 ± 0.02, which is attributed to the presence of HPMC for the encapsulation of the NPs.

Attenuated total reflectance Fourier transform infrared (ATR–FTIR) spectroscopy of the samples (Figure 1c) showed the chemical modifications taking place at the surface of the UnPSi at different steps of preparation. The surface of UnPSi was chemically modified with albumin via chemical conjugation between the activated carboxylic group of UnPSi and the free amine groups of albumin, in order to form amide bonds using carbodiimide crosslinker chemistry. The successful conjugation of albumin, already suggested by the alteration in the surface charge of the particles, was confirmed by the amide I band of albumin shift to 1647 cm^{-1} in the Alb-UnPSi, while the carbonyl C=O stretching of UnPSi at 1704 cm^{-1} is attenuated. The appearance of $–NH_2$ band at 1529 cm^{-1} also confirms the presence of amine groups in the Alb-UnPSi NPs. Upon encapsulation, the characteristic bands of HPMC appear in the spectra, confirming the presence of the polymer in the developed nanosystem.

The amount of albumin covalently conjugated to the surface of UnPSi NPs was quantified by elemental analysis (**Table S1**). Bare UnPSi NPs were used as control. The increased amount of elements C and H supports the successful functionalization of the NPs. Importantly, the

appearance of N element upon functionalization also suggests the presence of albumin (rich in primary amines) on the surface of the NPs, containing 1.70 ± 0.08 nmol of albumin on the surface of 1 mg of the UnPSi NPs.

The morphological characteristics and elemental composition of the nanosystem was further evaluated by TEM imaging and energy dispersive X-ray spectroscopy (EDX). TEM images showed the successful formation of Alb-UnPSi encapsulated in HPMC (Figure 1d). Images of the core UnPSi and Alb-UnPSi NPs can be found in **Figure S1**. The EDX elemental composition analysis confirmed that PSi NPs are inside of the polymer by the appearance of the Si peak in the spectra (Figure 1e, blue arrow), while Si atoms were not detected in bare HPMC particles (Figure 1e, black arrow). The measurement points for Alb-UnPSi@HPMC and bare HPMC are shown in **Figure S2**.

Overall, the physicochemical characterization of the NPs suggests a successful preparation of the Alb-UnPSi@HPMC nanosystem, with tunable size and size distribution, surface charge, and with prominent changes after surface modifications. TEM and EDX analysis further support the successful preparation of albumin-decorated UnPSi encapsulated with HPMC.

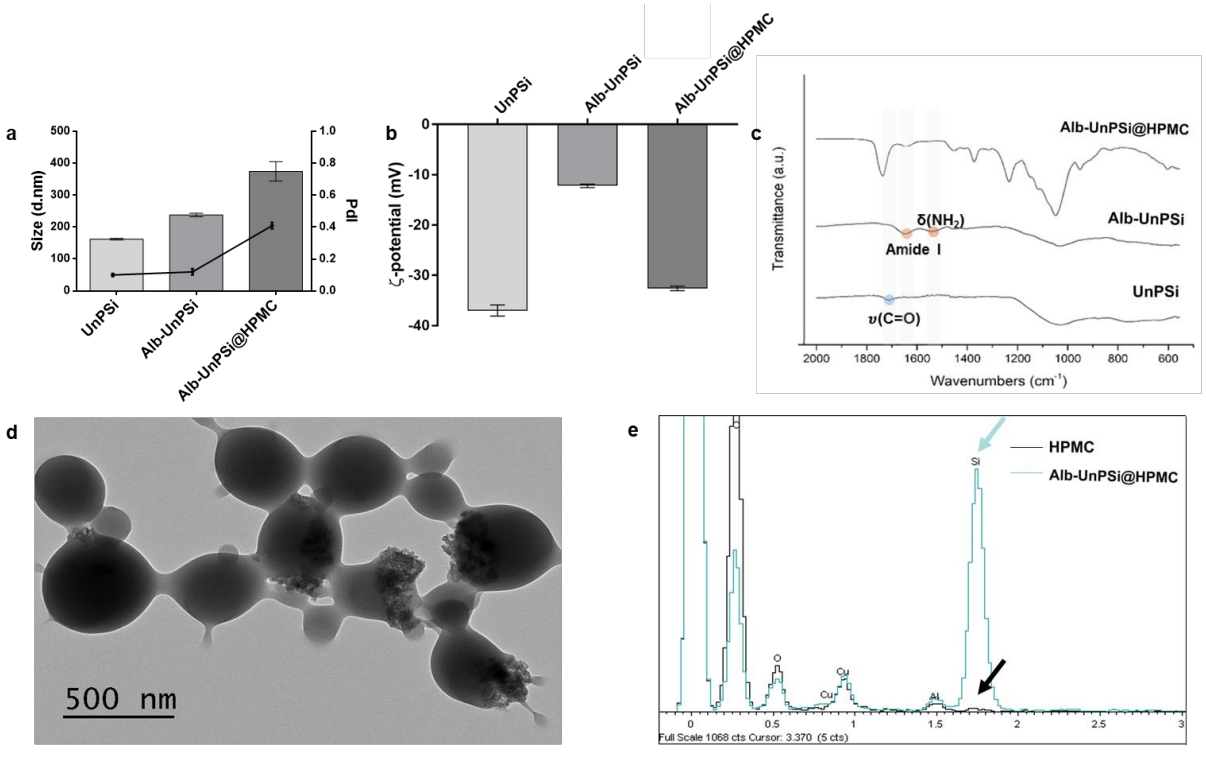

Figure 1. Physicochemical characterization of the prepared NPs. (a) Hydrodynamic diameter and PdI, (b) ζ-potential, and (c) ATR–FTIR spectra of UnPSi, Alb-UnPSi and Alb-UnPSi@HPMC. Results are represented as mean ± s.d. ($n \geq 3$). (d) TEM images of Alb-UnPSi@HPMC. (e) Elemental composition of bare HPMC and Alb-UnPSi@HPMC NPs by EDX analysis, showing the Si element (blue arrow) in the final nanosystem.

2.2. Drug loading and *in vitro* pH-responsive drug release studies

Insulin was loaded into the NPs by an immersion method after functionalization with albumin and prior to encapsulation into the HPMC polymeric matrix.[22, 24] The drug association efficiency and loading degree of the Alb-UnPSi@HPMC were 12 ± 2 % (w/w) and 0.70 ± 0.15 % (w/w), respectively. To evaluate the insulin release profile of the final formulation and, importantly, to study their fate in the gastrointestinal tract, the NPs were exposed to simulated gastric fluid (SGF, pH 1.2, without pepsin) for 2 h, followed by exposure to fasted stated simulated intestinal fluid (FaSSIF, pH 6.5) for the next 6 h. The duration and media used in this experiment were chosen according to the estimated gastric and intestinal residence times and pH.[26] To make sure that the insulin structure would not be compromised by the use of FaSSIF as simulated intestinal fluid, we firstly incubated insulin with FaSSIF for 6 h (**Figure S3**). Insulin in FaSSIF immediately after preparation was analyzed as control. UV-Vis spectra showed absorbance peaks for insulin in FaSSIF immediately after preparation and after 6 h in solution at 222 and 221 nm, respectively (Figure S3). Also, the concentration of insulin at the beginning of the experiment was 97.21 ± 0.68 ug mL^{-1}, and after 6 h incubation was 100.08 ± 1.57 ug mL^{-1}. The maintenance of insulin concentration over time suggests that insulin was not degraded upon exposition to FaSSIF for 6 h. No distinct peak was observed for FaSSIF alone, suggesting that the absorbance peaks observed in the UV-Vis derive exclusively from the presence of insulin in solution.

The release profiles of insulin from UnPSi and Alb-UnPSi@HPMC are shown in **Figure 2**. UnPSi non-protected by the HPMC were used as control. Results showed insulin release from the UnPSi NPs immediately in SGF, with an increase up to *ca.* 50% in FaSSIF. By contrast, the

final nanosystem showed no insulin release for the first 2 h in SGF, as expected by the intact form of the HPMC at this pH. However, when these NPs were moved to FaSSIF, a burst release was observed, with gradual release of insulin up to *ca.* 30% during the next 6 h. This effect is attributed to the pH-responsive properties of HPMC, which starts to degrade at intestinal pH. The release of insulin obtained at the end of the experiment was higher for the nanosystem without HPMC, but the absence of the pH-sensitive polymer and subsequent prolonged exposure to harsh stomach conditions might have a major impact on the integrity of the antidiabetic drug. Moreover, the release profile from Alb-UnPSi@HPMC was still increasing after 6 h, while from the UnPSi NPs a slight decrease was observed, suggesting degradation of the drug. The fact that not all the drug associated to the NPs was released can be attributed to the interactions between the hydrophobic regions of insulin and the hydrophobic pore surface of UnPSi NPs.[27] The layer of protein irreversibly adsorbed onto the pores of the NPs can therefore explain the incomplete release of insulin from the particles.

The *in vitro* release profile suggests successful association of insulin to the NPs and a controlled release under simulated stomach and intestinal conditions. The integrity of the insulin molecule when loaded into Alb-UnPSi@HPMC can be preserved due to the intact form of HPMC at acidic pH, being successfully released at intestinal conditions. The successful use of PSi as drug carrier, together with the albumin functionalization for targeting, and the entrapment of the NPs into a pH-responsive matrix turn this into a multifunctional system with potential to be tested *in vitro* for enhanced therapeutic effect of insulin after oral administration.

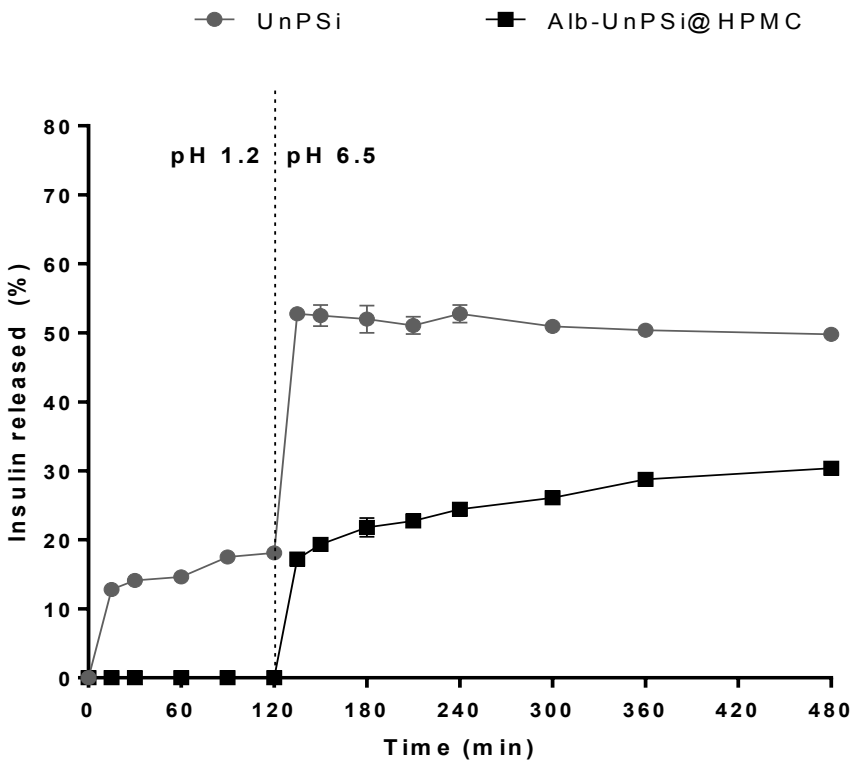

Figure 2. Release profiles of insulin from UnPSi and Alb-UnPSi@HPMC. The percentages of insulin released from non-encapsulated and HPMC encapsulated NPs were compared at the same time points. The experiments were conducted in SGF (pH 1.2) for the first 2 h, and then in FaSSIF (pH 6.5) for the remaining 6 h, at 37 °C and 100 rpm. Results are represented as mean ± s.d. (n = 3).

2.3. Cellular cytocompatibility studies

The cytocompatibility of the developed nanosystem in intestinal cell lines was evaluated by CellTiter-Glo® luminescence assay. C2BBe1 (clone of human colonic adenocarcinoma; Caco-2) cells were used to represent the enterocytes due to their greater degree of similarity when compared to cells isolated from the human colonocyte,[28] and the goblet-like cells (HT29-MTX) were used as mucus producing cells. In order to evaluate the highest non-toxic concentration of NPs to be used in the following studies, both cell lines were exposed to different concentrations of UnPSi, Alb-UnPSi, and Alb-UnPSi@HPMC particles, ranging from 25–200 μg mL^{-1}, for 12 and 24h. The quantification of the ATP content in metabolically active cells was performed using a validated luminescent method.[29] The percentages of viable cells

upon exposure to different concentrations of the different NPs for both cell lines and at different time points are presented in **Figure 3**.

Bare UnPSi NPs showed a concentration-dependent toxicity on both cell lines and time points, with increased toxicity upon increased concentration of particles. The Alb-UnPSi NPs showed cell viabilities higher than 80% after 24 h for both cell lines, indicating enhanced cytocompatibility when compared to the bare UnPSi NPs. This effect can be attributed to the biocompatibility of albumin attached to the surface of the UnPSi NPs, which is well-known for its lack of toxicity, antigenicity and ability to be degraded into innocuous natural products.[16] Cell viabilities over 80% were obtained for Alb-UnPSi@HPMC at all concentrations when in contact with C2BBe1 up to 24h, reinforcing the cytocompatibility of the developed nanosystem when encapsulated in this polymer.

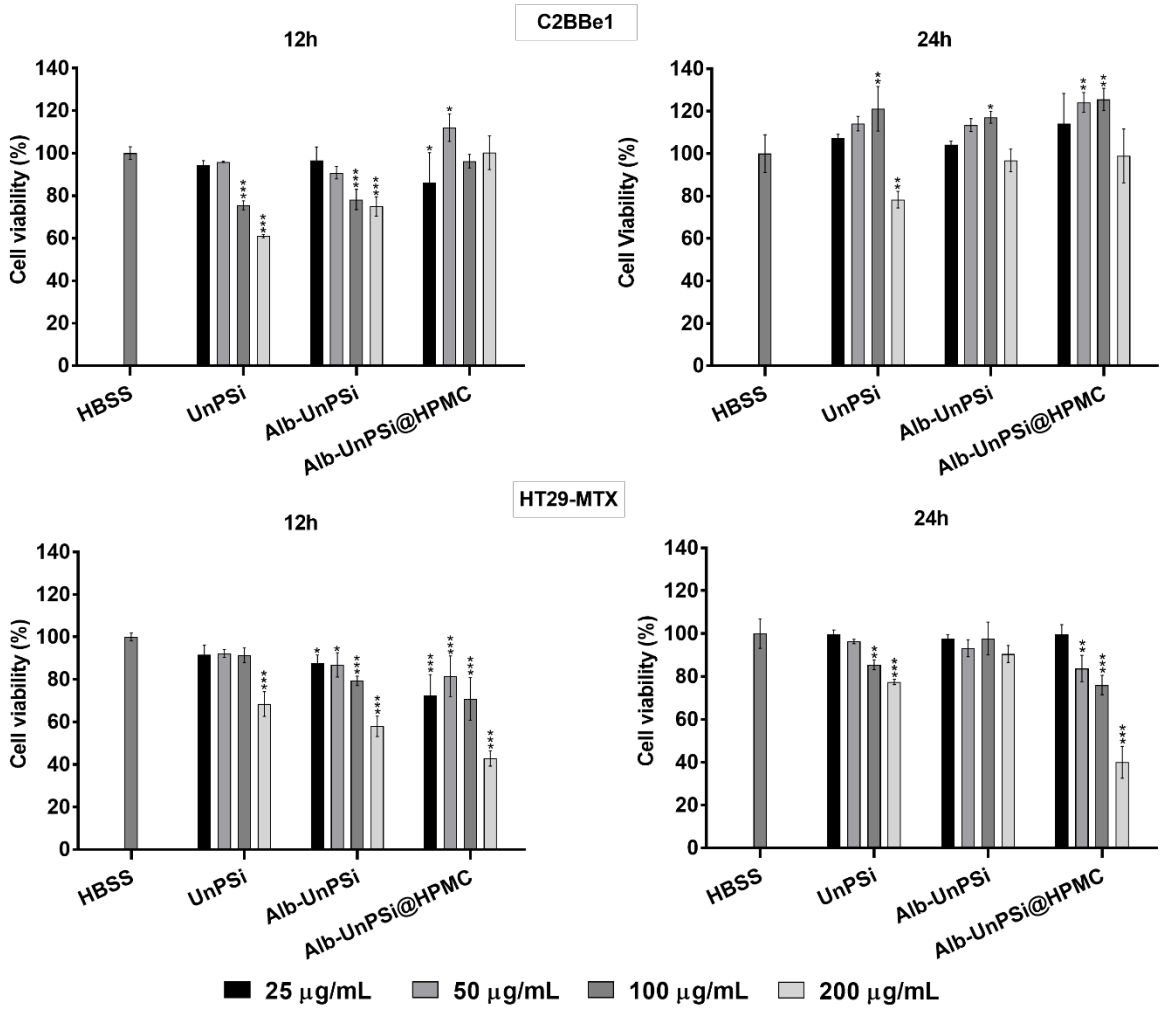

Figure 3. Cell viability of the intestinal cells exposed to UnPSi, Alb-UnPSi and Alb-UnPSi@HPMC NPs assessed by CellTiter-Glo® luminescence assay. The ATP content of C2BBe1 (12 and 24 h) and HT29-MTX (12 and 24 h) after the incubation with the different NPs at different concentrations was investigated. The NPs were incubated with the cells at 37°C in a humidified atmosphere. Statistical analysis was made by two-way ANOVA followed by Bonferroni post-test. All the data sets were compared to the negative control (HBSS–HEPES buffer; pH 7.4). The level of significance was set at probabilities of $*p < 0.05$, $**p < 0.01$ and $***p < 0.001$. Results are represented as mean ± s.d. ($n \geq 3$).

2.4. Validation of the *in vitro* intestinal model

In vitro models are essential for predicting the transport rate of a drug or molecule across the intestinal epithelium. In the present study, the use of an adequate *in vitro* model also plays a crucial role for a proper understanding of the behavior of the NPs when in contact with the intestinal microenvironment. Therefore, C2BBe1 and HT29-MTX cells were cocultured in a ratio of 90:10 for 21 days in Transwell™ membranes.[30] The functionality of the intestinal model established in this study was validated through the successful development of tight junctions observed by immunocytochemistry (**Figure S4**) and high transepithelial electrical resistance (TEER) values obtained at the end of the culture period (**Figure S5**). Also, the expression of the target receptor FcRn was evaluated by immunostaining and flow cytometry.

2.4.1. FcRn expression

FcRn can be found on the surface of epithelial cells, among others, working as a dual binding receptor that transports IgG and albumin across the intestinal epithelium, ensuring their homeostatic regulation.[16] Upon binding of IgG or albumin to the FcRn, an intracellular protein reservoir is created, protecting the binding molecules from lysosomal degradation and trafficking them across the cell.[16] Thus, IgG and albumin can act as taxi-molecules for cell transcytosis. The exploitation of this property turns albumin into one of the most attractive candidates for drug half-life extension, targeted intracellular drug delivery or increased transport of drugs with poor intestinal absorption, by methods of covalent conjugation, genetic fusions, association or ligand-mediated association.[31]

However, to our knowledge, no *in vitro* cellular studies have demonstrated so far whether FcRn can transport albumin-associated nanoparticles efficiently or not. Additionally, unlike parent Caco-2, which are known for endogenously expressing human FcRn,[32, 33] no studies have demonstrated the expression of FcRn in C2BBe1 cells. Similarly, the FcRn is reported to be expressed in HT29 cells,[34] but no studies have demonstrated whether the HT29-MTX cells can express this receptor. HT29-MTX cells are treated with methotrexate for exhibiting an entirely differentiated goblet cell-like phenotype.[35] When cocultured with C2BBe1, HT29-MTX cells can generate a mucus layer and overall increased permeability, therefore mimicking more accurately the *in vivo* scenario.[36] For these reasons, in the present study, FcRn expression in the *in vitro* C2BBe1/HT29-MTX coculture model was characterized by confocal microscopy and flow cytometry. The two cell lines were cocultured in ratio of 90:10, respectively, and treated with Alexa Fluor® 488-labeled human IgG Fc fragment. Immunocytochemistry showed that FcRn was expressed in the intestinal model, by the green fluorescence corresponding to the Alexa Fluor® 488-labeled human IgG Fc fragment, which is binding the FcRn (**Figure 4**). The quantitative flow cytometry results show a number of positive events corresponding to 4.1 ± 0.8 % (**Figure S6**). However, this value is significantly lower compared to a recent study reporting surface FcRn expression occurring in 62% of the total population of dissociated cells when using parent Caco-2 exposed to an in-house generated anti-FcRn antibody.[33] Nevertheless, this experiment demonstrated that the receptor is expressed on the *in vitro* coculture model used for the present study.

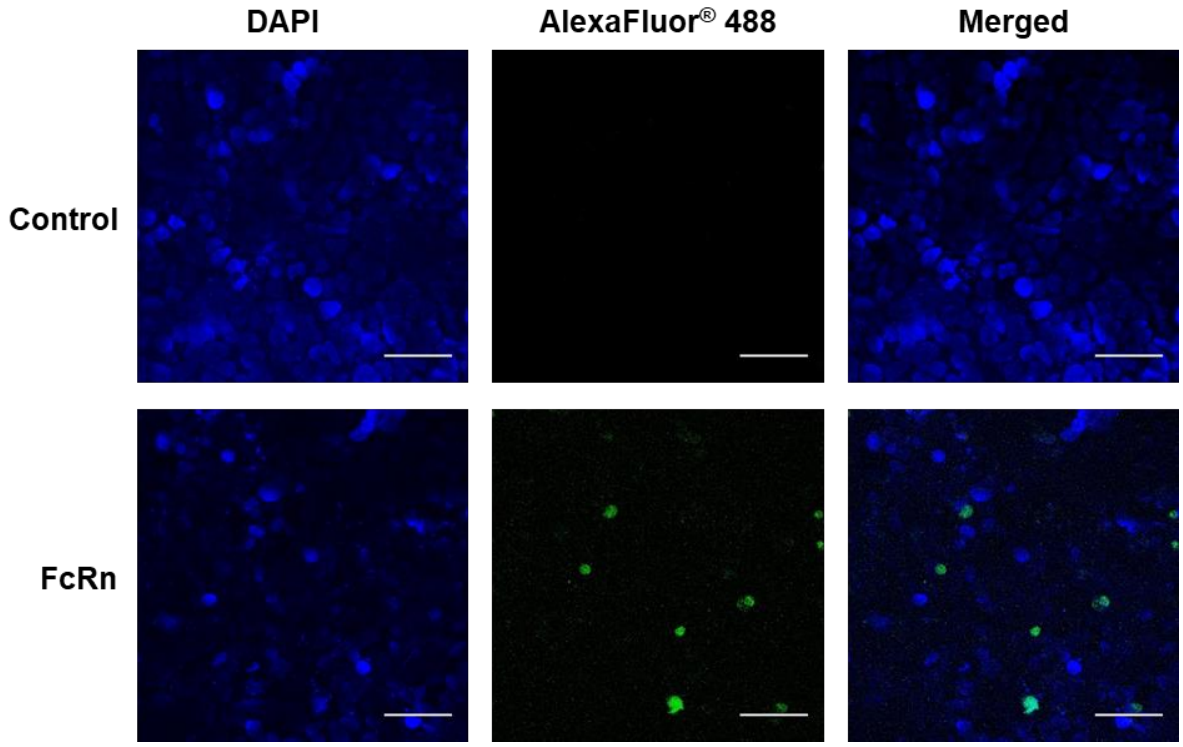

Figure 4. FcRn expression in the *in vitro* model. Confocal imaging microscopy of fixed C2BBe1/HT29-MTX cocultured for 21 days in Transwell™ filters after incubation with Fc fragment Alexa Fluor 488® conjugated (3.96 µg mL^{-1}) for 3h at 37 °C in humidified atmosphere. FcRn is stained with Fc fragment (in green) and nuclei with DAPI (in blue). Cocultures non-treated with Fc fragment were used as control. Scale bar is 50 µm.

2.5. Study of the cell–NP interactions

A C2BBe1/HT29-MTX coculture in a ratio of 90:10, respectively, was used as a reliable model to predict the behavior of the developed nanoparticles when in close contact to the intestinal cells.[30] Cell cultures were exposed to UnPSi@HPMC with and without albumin conjugation, in order to evaluate the impact of the presence of albumin as an FcRn-binding ligand when in contact with the cells. The experiment was conducted at intestinal pH, in which the HPMC is dissolved, exposing the core particles to the cells. After exposure to the different formulations, the cell cultures were washed multiple times, to remove the particles that are non-specifically interacting with the monolayers. Confocal microscopy and flow cytometry were used to assess the interaction between the NPs and the cells. The NPs were labeled with Alexa Fluor 488® conjugated by EDC/NHS chemistry for visualization and quantification purposes. In the

confocal images, the NPs are represented by green fluorescence, whereas the cell membranes, stained with CellMask™ Deep Red, are represented by red fluorescence.

Confocal images show minimal interaction of UnPSi@HPMC NPs in the absence of albumin (**Figure 5**). By contrast, a high rate of interaction was observed when using Alb-UnPSi@HPMC NPs, suggesting the specific interaction of the particles with FcRn (Figure 5). The possible yellow fluorescence observed in the images results from the overlapping of the green and red fluorescence, revealing a very close contact of the NPs with the cell membranes, where FcRn is located. No green fluorescence was detected in the cocultures that were not exposed to NPs, confirming that the green fluorescence derives from the Alexa Fluor 488®-labeled particles. In order to evaluate the specific interaction of the NPs with each cell type, C2BBe1 and HT29-MTX monocultures were individually incubated with the nanosystems. In the case of C2BBe1 cells, a similar cell-NP interaction pattern was observed (**Figure S7**), with minimal interaction of the particles in the absence of the FcRn ligand, which is increased upon the addition of albumin to the surface of the NPs. By contrast, a smaller difference between the cell–NP interactions was observed in HT29-MTX monocultures when exposed to UnPSi@HPMC and Alb-UnPSi@HPMC NPs (**Figure S8**). This can be explained by the presence of the mucus layer on the cell surface, increasing the electrostatic interaction of the NPs with the cells, regardless of the presence of albumin.

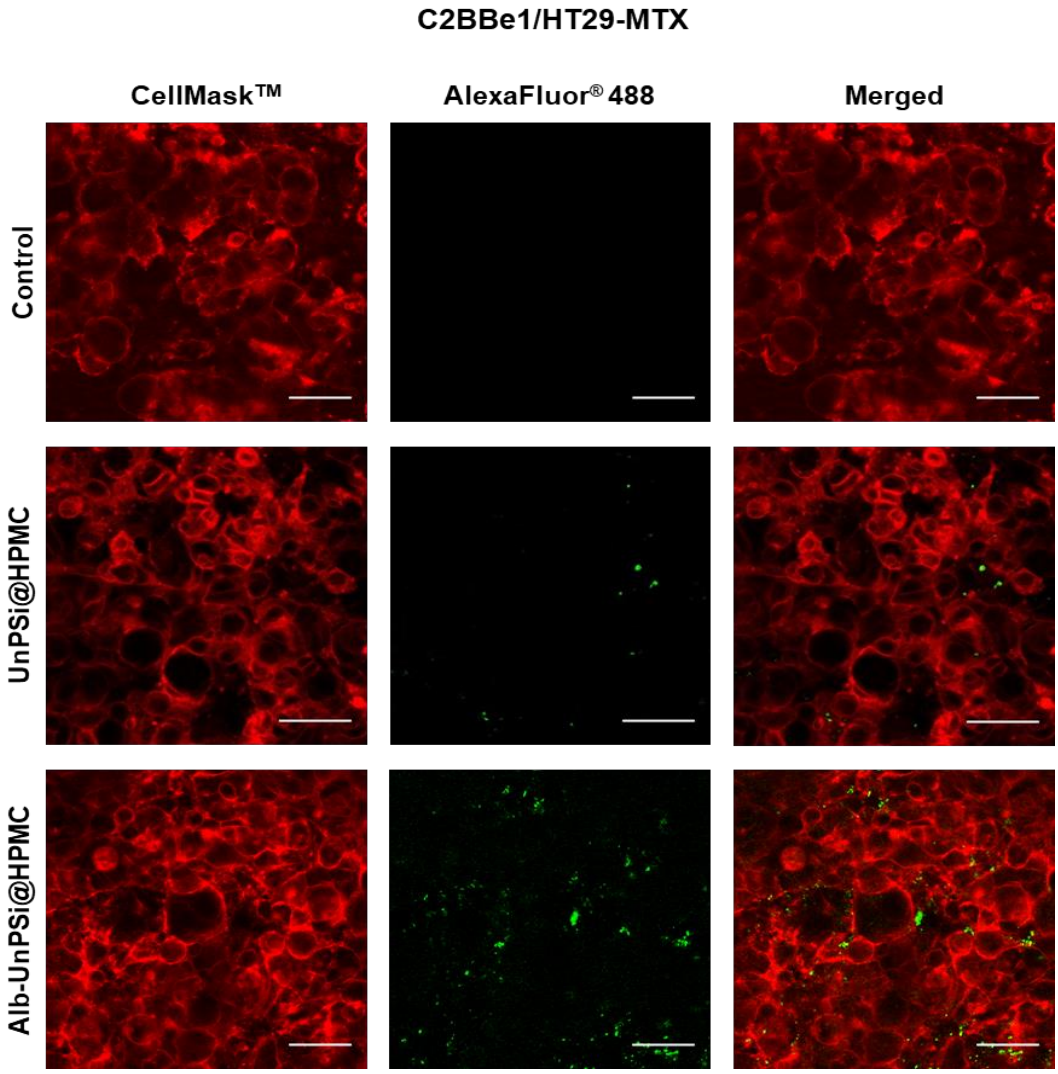

Figure 5. Interaction of the developed NPs with intestinal cells. Confocal microscopy imaging of C2BBe1/HT29-MTX cocultures incubated with UnPSi@HPMC functionalized and non-functionalized with albumin for 3 h at 37 °C. Cell membranes were stained with CellMask™ Deep Red (red); different NPs were labeled with Alexa Fluor® 488 (green).

To further investigate these results, the interaction of the different NPs with the intestinal cells was quantified by flow cytometry (**Figure 6**). Accordingly, C2BBe1/HT29-MTX cocultures were incubated with albumin-modified and non-modified UnPSi@HPMC, and the cell–NP interactions were recorded. Results are in accordance with the confocal images, showing a clear shift of the peak in the flow cytometry histogram of Alb-UnPSi@HPMC NPs (median fluorescence intensity, MFI = 637 ± 38) compared to UnPSi@HPMC (MFI = 180 ± 36) This indicates, therefore, increased interaction of albumin decorated NPs with the cells as compared to non-functionalized PSi NPs.

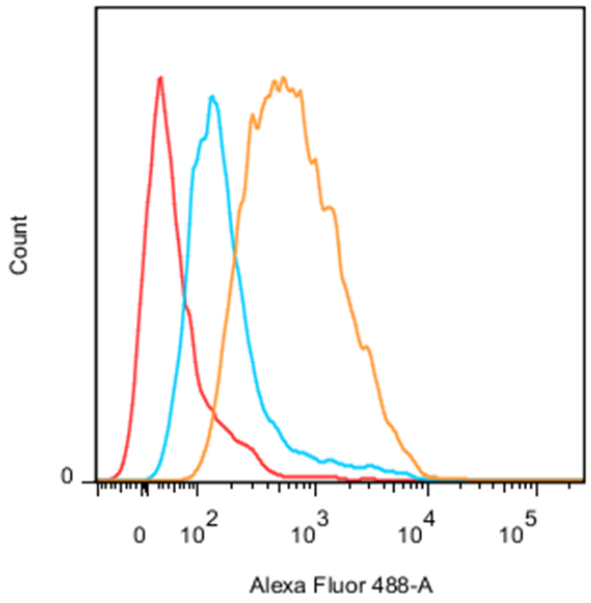

	MFI (a.u.)
C2BBe1/HT29-MTX	27.85 ± 3.55
UnPSi@HPMC	180 ± 35.86
Alb-UnPSi@HPMC	637 ± 37.67

Figure 6. Flow cytometry quantitative analysis of C2BBe1/HT29-MTX coculture (red) upon incubation with UnPSi@HPMC (blue) and Alb-UnPSi@HPMC (orange) for 3 h at 37 °C. The table summarizes the median fluorescence intensity (MFI) for each sample. Approximately, 10,000 events were counted for each measurement. Values represent the mean ± s.d. ($n \geq 3$).

Overall, high cellular association was observed in the intestine epithelium upon the presence of albumin in the surface of the PSi NPs, which is specific to the exposure to the FcRn expressing intestinal cells, suggesting their specific interaction with FcRn.

2.6. FcRn-targeted NPs for efficient insulin permeation across C2BBe1/HT29-MTX monolayers

After the promising data obtained from the cell–NP interaction studies, insulin permeability across the intestinal epithelium was studied to evaluate the efficacy of the proposed formulation in terms of drug transport. As suggested by the immunostainings of the tight junctions (Figure S4), the TEER values (Figure S5), and the FcRn expression (Figure 4; Figure S6), the C2BBe1/HT29-MTX coculture model resembles the most important features of the intestinal epithelium and it was therefore used as intestinal model for this experiment. Here, in contrast to the preliminary cell–NP interaction studies in which cells were cultured overnight, the cocultures were seeded in Transwell™ filters, and let to grow for 21 days, to allow for the

development of a polarized monolayer with fully differentiated cells.[30] Importantly, the expression of FcRn in normal Caco-2 cells is reported in the literature to vary according to their differentiation process,[37] and the same variation pattern is expected to happen also for the C2BBe1 cells. Therefore, one should take this into consideration when establishing a direct correlation between the cell–NP interaction studies and the insulin permeation results. Additionally, acidic and neutral pH buffers were used in the apical and basolateral compartments of the Transwell™, respectively, to mimic the conditions of the different sections of the intestine. This goes in accordance with the hypothesis that albumin would bind to FcRn in the acidic fragments of the intestine (apical surface of absorptive epithelial cells), then leading to receptor-mediated endocytosis.[15] Albumin-decorated NPs would then be transported across the cells through a transcytotic pathway, and then exocytosed in the basolateral compartment, where a neutral pH can be found.[15]

The cumulative permeability (%) profiles obtained showed that the capacity of free insulin to permeate the intestine revealed to be highly limited, as expected by the presence of tight junctions and the protective mucus layer.[38] In turn, the permeation of insulin loaded in the non-targeted NPs was higher when compared to pure insulin (**Figure 7**). The use of UnPSi NPs might have promoted a slight increase in the permeability across the cell monolayer. A significant increase (*ca*. 5-fold; $p < 0.0001$) in the amount of insulin that permeated the epithelium was achieved upon exposition of the cocultures to FcRn-targeted Alb-UnPSi@HPMC NPs, when comparing to UnPSi@HPMC or free insulin. The addition of albumin as FcRn-targeting ligand revealed to induce an increase in the transport of insulin across the monolayer. This can be explained by a synergistic effect promoted by the increase in the surface charge of the NPs of about 25 mV upon functionalization, which may slightly improve the mucoadhesion and prolong the cell–NP contact time, together with the increased drug release in the close vicinity of the cells, as previously reported,[39] and importantly, the FcRn transcytotic capacity. The fact that there is no increase in the insulin permeation after the

first 15 min might be related to the amount of drug that can be released from the NPs and, particularly, to the amount of NPs that can be used to perform the experiment, considering the limited area of a Transwell™ filter and the concentration of NPs that can be used without significant cytotoxicity. Additionally, to our knowledge, it is not reported in the literature the duration of a cycle of FcRn transcytosis, and therefore, it is not clear whether an increase on the insulin permeated is expected after that time. Nonetheless, *in vivo* studies will be crucial to determine the potential of the developed NPs in a living organism after oral administration. Such studies will demand the use of a human FcRn expressing transgenic mouse model, in which the deletion of the mouse FcRn avoids any influence of the endogenous expression of the receptor. Interestingly, the promotion of insulin permeation by the use of FcRn-targeted NPs observed *in vitro* or *in vivo* might be significantly enhanced in humans, which constitutively express FcRn in the intestinal epithelium.[40] The monitoring of the TEER values showed that the integrity of the monolayer was maintained intact during the experiment, supporting the significance of the obtained data (**Figure S9**).

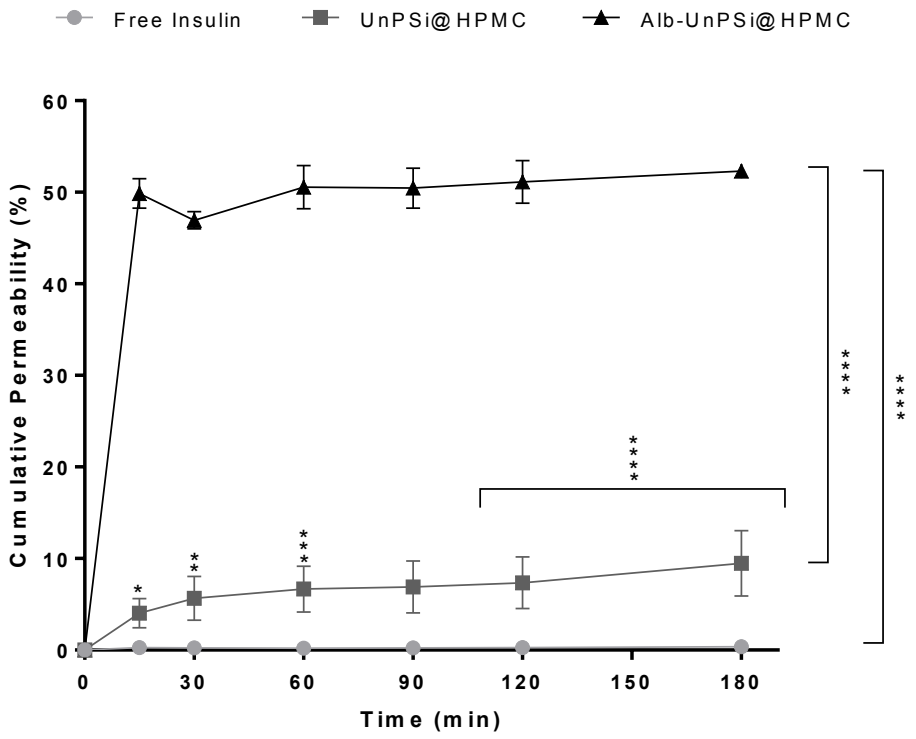

Figure 7. *In vitro* permeability profiles of free insulin and FcRn-targeted and non-targeted NPs loaded with insulin across C2BBe1/HT29-MTX monolayers. All experiments were conducted from the apical (pH 6.5) to the basolateral direction (pH 7.4) in HBSS–HEPES buffer at 37 °C. The level of significance was set at probabilities of $*p < 0.05$, $**p < 0.01$, $***p < 0.001$ and $****p < 0.0001$. Results are represented as mean ± s.d. ($n \geq 3$).

3. Conclusion

In this study, an engineered system aimed for oral administration of insulin for diabetes therapy was fabricated. Albumin-modified UnPSi NPs were used as the drug carriers for FcRn-targeting in order to increase transport of insulin across the intestinal cells. The formulation was rendered with a pH-responsive capacity by encapsulation of the core NPs into HPMC, with controlled size and size distribution for intestinal translocation. The NPs were efficiently encapsulated into pH-sensitive polymer, thereby preventing drug release and degradation in the harsh stomach environment, and a controlled and pH-responsive insulin release profile was achieved. Cytotoxicity studies showed high compatibility of the developed NPs with intestinal epithelial cells, while the *in vitro* insulin permeation across the intestinal epithelium revealed to be significantly enhanced when the drug was loaded into the albumin-decorated FcRn-targeted NPs. Overall, the advantageous PSi drug carrier properties, the pH-responsive capacity, and the FcRn targeting properties turn this into a multifunctional nanocarrier system. Moreover, the present work provides new insights in the underexplored FcRn-targeted therapies, and the advanced nanosystem proposed here shows great potential as a novel and multipurpose nanocarrier system for efficient FcRn-targeted insulin delivery.

4. Experimental Section

Materials: The list of materials and reagents used is reported in Supporting Information.

Preparation of undecylenic acid modified thermally hydrocarbonized porous silicon (UnPSi) nanoparticles: UnPSi NP were prepared as previously reported,[23, 24] and the detailed protocol is described in Supporting Information.

Conjugation of albumin to UnPSi NPs: 1-ethyl-3-(3-dimethylaminopropyl)-carbodiimide/N-hydroxysuccinimide (EDC/NHS) chemistry was used for the covalent conjugation of albumin to the surface of the UnPSi NPs. Briefly, 1 mg of NPs were dispersed in 2.7 mL of 2-(*N*-morpholino-ethanesulfonic acid (MES) buffer and tip-sonicated for 30 s using a Vibra-Cell™ ultrasonic processor (Sonics®, Sonics and Materials, Inc., USA). 5.33 µL of EDC and 4 mg of NHS were added to the solution, the pH was adjusted to 5.2, and stirred for 2 h, at RT in dark conditions, to activate the carboxylic groups on the surface of the UnPSi NPs. Afterwards, the particles were centrifuged, the supernatant was discarded, and the particles were again dispersed in 958 µL of MES buffer at pH 7.2, containing 17.5 µL of human albumin (5.7 mg mL^{-1}). The particles were again tip-sonicated for 10 s and the dispersion was stirred for 6 h to allow for chemical conjugation. Then, the NPs were washed two times with MilliQ-water to remove the excess of albumin, as reported elsewhere.[23]

Loading of insulin into UnPSi NPs: Insulin-loaded UnPSi NPs were prepared by an immersion method, as previously reported.[22, 24] Briefly, 1 mg of NPs were dispersed in 500 µL of Milli-Q water and then immersed in 2.25 mL of insulin solution (200 µg mL^{-1} in 0.01 M HCl). The solution was stirred and maintained at RT for 90 min. Afterwards, the excess amount of insulin was removed by centrifugation at 27,600× g (Optima MAX, Beckmann Coulter, USA), and the particles were washed once with Milli-Q water.

Encapsulation of Alb-UnPSi NPs into pH-sensitive polymer: The insulin-loaded albumin-conjugated NPs (Alb-UnPSi NPs) were encapsulated into HPMC, an enteric pH-sensitive

coating polymer, using modified emulsification-evaporation method, based on the water-in-oil-in-water (w/o/w) double emulsion technique. Briefly, the Alb-UnPSi NPs were dispersed in 100 µL of MilliQ-water and added to 2 mL of HPMC in ethyl acetate (25 mg mL^{-1}). The solution was sonicated for 10s to form the primary emulsion (w/o). Then, 100 µL of the particle solution was dropwise added to 500 µL of MilliQ (pH < 5), and sonicated for 10 s, forming the second emulsion (w/o/w). Finally, the Alb-UnPSi NPs encapsulated in HPMC (Alb-UnPSi@HPMC) were transferred to 1% PVA in MilliQ water (pH 4.7) and left under magnetic stirring for at least 2 h for organic solvent evaporation.

Particle characterization: The NPs were characterized for their average particle size (*z*-average), polydispersity index (PdI), and zeta-potential (ζ-potential) using Malvern Zetasizer Nano instrument (Malvern Ltd., UK).

Surface chemical modifications (human albumin conjugation, and HPMC encapsulation) were characterized by attenuated total reflectance Fourier transform infrared (ATR–FTIR) using a Bruker VERTEX 70 series FTIR spectrometer (Bruker Optics, Germany) with a horizontal ATR sampling accessory (MIRacle, Pike Technology, USA). The NPs were left to dry at RT before the measurements with a resolution of 4 cm^{-1}. The amount of albumin covalently conjugated to the surface of the UnPSi NPs was determined by elemental analysis using a Vario Micro cube CHN analyzer (Elementar Analysensysteme, GmbH, Germany) in dry samples. The percentages of carbon (C), hydrogen (H), nitrogen (N), and sulfur (S) were recorded. The amount of albumin on the surface of the NPs was calculated based on the percentage of each element and the chemical structure of albumin.

The morphology of the different NPs was assessed by transmission electron microscopy (TEM, Tecnai™ F12, FEI Company, USA). For this purpose, the particles were dispersed in water and then placed over copper-coated grids. The grids were dried at RT before imaging with TEM.

The elemental compositions of Alb-UnPSi@HPMC and bare HPMC NPs were measured using Oxford INCA 350 energy dispersive X-ray spectrometer (EDX) connected with a field emission scanning electron microscope (FESEM; Hitachi S-4800, Japan). The measurement points were selected from areas imaged with the bright field TE detector of the FESEM.

Association efficiency (AE) and loading degree (LD): AE and LD were calculated to determine the amount of insulin associated to the produced nanoparticles. Insulin AE (%) and LD (%) were determined according to the following equations (1) and (2):

$$AE\ (\%) = \frac{Initial\ amount\ of\ insulin\ added\ (\mu g) - Free\ unloaded\ drug\ (\mu g)}{Initial\ amount\ of\ insulin\ added\ (\mu g)} \times 100 \quad (1)$$

$$LD\ (\%) = \frac{Initial\ amount\ of\ insulin\ added\ (\mu g) - Free\ unloaded\ drug\ (\mu g)}{Total\ mass\ of\ NPs\ (\mu g) + Total\ mass\ of\ polymer\ (\mu g)} \times 100 \quad (2)$$

The amount of insulin was investigated using high performance liquid chromatography (HPLC; Agilent 1 260, Agilent Technologies, USA) and a C_{18} column (4.6 × 150 mm, 5µm, Supelco Discovery®, USA). For the HPLC detection, the mobile phase consisted of acetonitrile (ACN) and 0.1 trifluoroacetic acid (TFA) (pH 2.0), under a gradient system. The initial ratio of ACN and 0.1% TFA was 20:80 (v/v), which was changed to 30:70 (v/v) during 7 min, and then changed back to 20:80 (v/v) for the next 3 min. The flow rate was 1.2 mL min^{-1} and the injected volume of the sample was 50 µL. The column temperature was set to RT and the detection wavelength was 240 nm. The total area under the curve (AUC) was used to quantify the insulin.

UV-Visible spectroscopy: The UV-Vis spectra of insulin in FaSSIF was measured immediately after dissolution and after 6 h incubation of the drug using a UV-1600PC spectrophotometer (VWR, Radnor, PA, USA). Insulin initial concentration in both solutions was 100 µg mL^{-1}.

In vitro release studies: The *in vitro* insulin release profile of Alb-UnPSi@HPMC was performed in simulated gastric fluid (SGF) without pepsin (0.2% w/v sodium chloride, 0.7% (v/v) hydrochloric acid, pH 1.2), and in fasted state simulated intestinal fluid (FaSSIF, 50 mM dihydrogen sodium phosphate, 8.7 mM sodium hydroxide, dichloromethane, sodium taurocholate, and L-α-phosphatidylcholine, pH 6.5), to better mimic the passage of the NPs throughout the gastrointestinal tract. Insulin release from UnPSi was performed as control. The amount of NPs equivalent to 35 μg of insulin was dispersed in 10 mL SGF for 2 h to investigate the release of the drug in gastric conditions. SGF without pepsin was used to avoid discrepancies caused by insulin degradation in the presence of this enzyme. After 2 h, the NPs were removed from SGF by centrifugation, re-dispersed in 10 mL of FaSSIF and the insulin release was evaluated for the following 6 h. The insulin release was performed at 37 ˚C and magnetic stirring at 300 rpm. 500 μL samples were withdrawn at different time points until 480 min, and replaced with pre-warmed solutions (SGF or FaSSIF) to maintain the release volumes. The collected samples were centrifuged at 27, 600× g, and the supernatants were analyzed in HPLC.

Cell lines and culture conditions: C2BBe1 (clone of human colon adenocarcinoma Caco-2) was obtained from the American Type Culture Collection (ATCC, USA). Human goblet-like HT29-MTX was kindly provided by Dr. T. Lesuffleur (INSERM U178, Villejuif, France). C2BBe1 (passages #57–69) cells and HT29-MTX (passages #27-35) were grown separately in tissue culture flasks (Corning Inc., USA) in DMEM medium supplemented with 10% (v/v) heat inactivated fetal bovine serum (FBS), 1% (v/v) L-glutamine, 1% (v/v) NEEA and 1% (v/v) antibiotic–antimitotic mixture (final concentration of 100 IU ml^{-1} Penicillin and 100 IU ml^{-1} Streptomycin). The cells were maintained in an incubator (16 BB gas, Heraeus Instruments GmbH, Germany) at 37 °C and 5% CO_2 in a water saturated atmosphere. Growing medium was

changed every other day for the two cell lines. Sub-culturing was performed at 80% confluency. Cells were passaged using trypsin-PBS-EDTA.

Cytotoxicity assay: Cell viability experiments were conducted using C2BBe1 and HT29-MTX cells separately. Cells were seeded at concentration of 5×10^4 cells per mL into 96-well plates (Corning Inc., USA), and allowed to attach for 24 h. Then, cell culture medium was removed and cells were washed twice with fresh HBSS–HEPES buffer (pH 7.4). After that, UnPSi NPs, Alb-UnPSi NPs and Alb-UnPSi@HPMC were added to the cells at concentrations of 25, 50, 100 and 200 μg mL^{-1} and incubated for 12 and 24 h in a humidified 5% CO_2 atmosphere at 37 ºC. At these time points, after washing twice with HBSS–HEPES buffer, 100 μL of fresh HBSS–HEPES buffer and CellTiter-Glo® reagent assay (ratio 1:1) were added to the wells. 1% Triton X-100 and HBSS–HEPES buffer solution were used as positive and negative controls, respectively. The luminescence was measured using Varioskan Lux Multimode Reader (ThermoFisher Scientific, USA). The experiments were carried out in triplicates ($n \geq 3$).

Immunostaining of tight junctions: The detailed protocol of the immunostaining of the tight junctions for the validation of the *in vitro* model is described in Supporting Information.

Transepithelial electrical resistance (TEER) measurements: The successful establishment of tight junctions was further evaluated by monitoring the TEER values of the cell culture model. The detailed protocol is described in Supporting Information.

FcRn characterization: This experiment was designed to determine the FcRn expression in the 2D *in vitro* cell culture model. C2BBe1/HT29-MTX cocultures were grown in insert membranes, as described above. After 20 days in culture, cells were incubated O/N in serum free medium to prevent occupation of the receptor with serum constituents. Experiments were

performed at day 21. C2BBe1/HT29-MTX cocultures were exposed to Alexa Fluor® 488-ChromPure Human IgG, Fc fragment (3.96 μg mL^{-1}) for 3 h in the incubator at 37 °C and 5% CO_2. For FcRn immunofluorescence, cells were washed extensively, and fixed using 4% PFA. Transwell™ filter membranes were cut and assembled with Vectashield® antifade mounting medium containing DAPI for nuclei counterstaining, and observed at Leica SP5 II HCS A confocal microscope (Leica Microsystems, Wetzlar, Germany). For flow cytometry, cells were washed after exposure to the Fc fragment, and dissociated with Accutase®. Cells were washed again and re-suspended in 700 μL of PBS (0.1 M), and analyzed in BD LSR II (BD Biosciences, San Jose, CA, USA). Controls for both immunofluorescence and flow cytometry techniques included the omission of the Fc fragment.

Cell-NP interaction studies: To further assess the interaction between the cells and the NPs, confocal fluorescence microscopy and flow cytometry were used as qualitative and quantitative studies, respectively. For this purpose, UnPSi NPs were fluorescently labelled with AlexaFluor® 488 using EDC/NHS chemistry prior to the albumin conjugation described above. For confocal microscopy studies, cocultures of C2BBe1 and HT29-MTX cells (ratio of 90:10, respectively) were seeded into Lab-Tek™ 8-chamber slides (Thermo Fisher Scientific, USA), at a concentration of 2×10^5 cells per mL, and maintained in a humidified atmosphere at 37 °C and 5% CO_2. C2BBe1 and HT29-MTX monocultures were used as control. After 24h, cells were extensively washed with HBSS–HEPES (pH 7.4), and 250 μg of NPs were added to the each chamber and allowed to incubate for 3 h at 37 °C. After the incubation, cells were washed twice with pre-warmed HBSS–HEPES (pH 7.4) to remove non-interacting particles. Cell membranes were stained with CellMask® DeepRed by incubation at 37 °C for 4 min. After washings, cells were immediately observed at Leica SP5 II HCS A confocal microscope (Leica Microsystems, Wetzlar, Germany). For flow cytometry studies, C2BBe1/HT29-MTX cocultures (ratio 90:10, respectively) were seeded at a concentration of 6.8×10^4 cells/cm^2, in

12-well plates, and incubated overnight in a humidified atmosphere at 37 °C and 5% CO_2. Afterwards, the cells were washed and incubated with the different NPs, following the same parameters used for the confocal studies. After post-incubation washings, cells were dissociated from the culture plates with Versene. Cells were washed again and re-suspended in 700 µL of PBS (0.1 M) for analysis in BD LSR II (BD Biosciences, San Jose, CA, USA).

In vitro permeability assay: For the *in vitro* permeability assay, C2BBe1/HT29-MTX cocultures were seeded and maintained for 21 days, as described above. At the end of the culture period, the permeability of insulin-loaded Alb-UnPSi@HPMC NPs across the cell monolayers was investigated from the apical (0.5 mL) to the basolateral direction (1.5 mL) in the Transwell™ filters, using HBSS-HEPES buffer solution (pH 6.5 and pH 7.4, respectively). Insulin-loaded NPs were added to the apical chamber, the equivalent amount of free insulin was also added as control. The plates were maintained at 37 °C and shaken at 100 rpm. At different time points (10, 30, 60, 90, 120 and 180 min), 200 µL samples were withdrawn from the basolateral chambers, and replaced with the exact same volume of pre-warmed HBSS–HEPES (pH 7.4), to maintain the volume of the medium. The concentrations of insulin that permeated the cell monolayers were measured using HPLC. TEER measurements were performed at every time point to assess the integrity of the monolayer throughout the experiment as described in Supporting Information.

Statistical analysis: The experiments were performed in triplicates and are represented as mean ± standard deviation. Two-way analysis of variance (ANOVA) with Bonferroni post-test were used to analyze the data. The levels of significance were set at probabilities of $*p < 0.05$, $**p < 0.01$, $***p < 0.001$, $****p < 0.0001$.

Supporting Information
Supporting Information is available from the Wiley Online Library or from the author.

Acknowledgements
B. Sarmento acknowledges the project NORTE-01-0145-FEDER-000012, supported by Norte Portugal Regional Operational Programme (NORTE 2020), under the PORTUGAL 2020 Partnership Agreement, through the European Regional Development Fund (ERDF). B. Sarmento also acknowledges financial support by FEDER - Fundo Europeu de Desenvolvimento Regional funds through the COMPETE 2020 - Operational Programme for Competitiveness and Internationalisation (POCI), Portugal 2020, and the Portuguese funds through FCT - Fundação para a Ciência e a Tecnologia/Ministério da Ciência, Tecnologia e Ensino Superior in the framework of the project "Institute for Research and Innovation in Health Sciences" (POCI-01-0145-FEDER-007274). H.A. Santos acknowledges financial support from the University of Helsinki Research Funds, the Biocentrum Helsinki, the Sigrid Jusélius Foundation (decision no. 4704580), the HiLIFE Research Funds, and the European Research Council under the European Union's Seventh Framework Programme (FP/2007-2013, grant no. 310892). The authors acknowledge the following core facilities funded by Biocenter Finland: Electron Microscopy Unity of the University for providing the facilities for TEM imaging, and the Light Microscopy Unit of the Institute of Biotechnology for the confocal microscope. Kaisa Hytti from Aalto University, Finland, is acknowledged for technical support for the elemental analysis measurements.

Conflict of Interest
The authors declare no conflict of interest.

Received: ((will be filled in by the editorial staff))
Revised: ((will be filled in by the editorial staff))
Published online: ((will be filled in by the editorial staff))

References

[1] P. Fonte, F. Araújo, C. Silva, C. Pereira, S. Reis, H. A. Santos, B. Sarmento, *Biotechnol. Adv.* **2015**, *33*, 1342.
[2] J. A. Bluestone, K. Herold, G. Eisenbarth, *Nature* **2010**, *464*, 1293.
[3] S. V. Sastry, J. R. Nyshadham, J. A. Fix, *Pharm. Sci. Technol. Today* **2000**, *3*, 138.
[4] M. A. Eaton, L. Levy, O. M. Fontaine, *Nanomedicine* **2015,** *11*, 983.
[5] X. Q. Zhang, X. Xu, N. Bertrand, E. Pridgen, A. Swami, O. C. Farokhzad, *Adv. Drug Deliv. Revb* **2012**, *64*, 1363.
[6] S. Martins, B. Sarmento, D. C. Ferreira, E. B. Souto, *Int. J. Nanomed.* **2007**, *2*, 595.
[7] F. Araújo, J. das Neves, J. P. Martins, P. L. Granja, H. A. Santos, B. Sarmento, *Prog. Mater. Sci.* **2017**, *89*, 306.
[8] L. M. Ensign, R. Cone, J. Hanes, *Adv. Drug Deliv. Rev.* **2012**, *64*, 557.
[9] K. Petrak, *Drug Discov. Today* **2005**, *10*, 1667.
[10] S. D. Steichen, M. Caldorera-Moore, N. A. Peppas, *Eur. J. Pharm. Sci.* **2013**, *48*, 416.
[11] D. A. Richards, A. Maruani, V. Chudasama, *Chem. Sci.* **2017**, *8*, 63.
[12] N. Shrestha, F. Araujo, M. A. Shahbazi, E. Mäkilä, M. J. Gomes, M. Airavaara, E. I. Kauppinen, J. Raula, J. Salonen, J. Hirvonen, B. Sarmento, H. A. Santos, *J. Control. Release* **2016**, *232*, 113.
[13] N. Shrestha, M.-A. Shahbazi, F. Araújo, H. Zhang, E. M. Mäkilä, J. Kauppila, B. Sarmento, J. J. Salonen, J. T. Hirvonen, H. A. Santos, *Biomaterials* **2014**, *35*, 7172.

[14] F. Araújo, N. Shrestha, M.-A. Shahbazi, P. Fonte, E. M. Mäkilä, J. J. Salonen, J. T. Hirvonen, P. L. Granja, H. A. Santos, B. Sarmento, *Biomaterials* **2014**, *35*, 9199.
[15] E. M. Pridgen, F. Alexis, T. T. Kuo, E. Levy-Nissenbaum, R. Karnik, R. S. Blumberg, R. Langer, O. C. Farokhzad, *Sci. Transl. Med.* **2013**, *5*, 213ra167.
[16] J. P. Martins, P. J. Kennedy, H. A. Santos, C. Barrias, B. Sarmento, *Pharmacol. Ther.* **2016**, *161*, 22.
[17] D. C. Roopenian, S. Akilesh, *Nat. Rev. Immunol.* **2007**, *7*, 715.
[18] D. Lalezari, *Ann. Gastroenterol.* **2012**, *25*, 333.
[19] K. S. Pang, *Drug Metab. Dispos.* **2003**, *31*, 1507.
[20] H. A. Santos, E. Mäkilä, A. J. Airaksinen, L. M. Bimbo, J. Hirvonen, *Nanomedicine (Lond)* **2014**, *9*, 535.
[21] L. M. Bimbo, M. Sarparanta, H. A. Santos, A. J. Airaksinen, E. Mäkilä, T. Laaksonen, L. Peltonen, V.-P. Lehto, J. Hirvonen, J. Salonen, *ACS Nano* **2010**, *4*, 3023.
[22] J. Salonen, A. M. Kaukonen, J. Hirvonen, V. P. Lehto, *J. Pharm. Sci.* **2008**, *97*, 632.
[23] N. Shrestha, M. A. Shahbazi, F. Araujo, E. Mäkilä, J. Raula, E. I. Kauppinen, J. Salonen, B. Sarmento, J. Hirvonen, H. A. Santos, *Biomaterials* **2015**, *68*, 9.
[24] M.-A. Shahbazi, N. Shrestha, E. Mäkilä, F. Araújo, A. Correia, T. Ramos, B. Sarmento, J. Salonen, J. Hirvonen, H. A. Santos, *Nano Res.* **2015**, *8*, 1505.
[25] D. T. Friesen, R. Shanker, M. Crew, D. T. Smithey, W. J. Curatolo, J. A. Nightingale, *Mol. Pharmaceutics* **2008**, *5*, 1003.
[26] D. M. Mudie, G. L. Amidon, G. E. Amidon, *Mol. Pharmaceutic* **2010**, *7*, 1388.
[27] N. Shrestha, F. Araújo, M.-A. Shahbazi, E. Mäkilä, M. J. Gomes, B. Herranz-Blanco, R. Lindgren, S. Granroth, E. Kukk, J. Salonen, J. Hirvonen, B. Sarmento, H. A. Santos, *Adv. Funct. Mater.* **2016**, *26*, 3405.
[28] M. D. Peterson, M. S. Mooseker, *J. Cell Sci.* **1992**, *102*, 581.
[29] H. A. Santos, J. Riikonen, J. Salonen, E. Mäkilä, T. Heikkilä, T. Laaksonen, L. Peltonen, V.-P. Lehto, J. Hirvonen, *Acta Biomater.* **2010**, *6*, 2721.
[30] F. Araujo, B. Sarmento, *Int. J. Pharm.* **2013**, *458*, 128.
[31] M. T. Larsen, M. Kuhlmann, M. L. Hvam, K. A. Howard, *Mol. Cell Ther.* **2016**, *4*, 3.
[32] M. Yoshida, S. M. Claypool, J. S. Wagner, E. Mizoguchi, A. Mizoguchi, D. C. Roopenian, W. I. Lencer, R. S. Blumberg, *Immunity* **2004**, *20*, 769.
[33] P. J. Hornby, P. R. Cooper, C. Kliwinski, E. Ragwan, J. R. Mabus, B. Harman, S. Thompson, A. L. Kauffman, Z. Yan, S. H. Tam, H. Dorai, G. D. Powers, J. Giles-Komar, *Pharm. Res.* **2014**, *31*, 908.
[34] B. L. Dickinson, K. Badizadegan, Z. Wu, J. C. Ahouse, X. Zhu, N. E. Simister, R. S. Blumberg, W. I. Lencer, *J. Clin. Investig.* **1999**, *104*, 903.
[35] M. Gagnon, A. Zihler Berner, N. Chervet, C. Chassard, C. Lacroix, *J.Microbiol. Meth.* **2013**, *94*, 274.
[36] S. M. Orbach, R. R. Less, A. Kothari, P. Rajagopalan, *ACS Biomater. Sci. Eng.* **2017**, *3*, 1898.
[37] K. Sato, J. Nagai, N. Mitsui, Y. Ryoko, M. Takano, *Life Sci.* **2009**, *85*, 800.
[38] O. Pillai, R. Panchagnula, *Drug Discov. Today* **2001**, *6*, 1056.
[39] L. M. Bimbo, M. Sarparanta, E. Mäakilä, T. Laaksonen, P. Laaksonen, J. Salonen, M. B. Linder, J. Hirvonen, A. J. Airaksinen, H. A. Santos, *Nanoscale* **2012**, *4*, 3184.
[40] E. J. Israel, S. Taylor, Z. Wu, E. Mizoguchi, R. S. Blumberg, A. Bhan, N. E. Simister, *Immunology* **1997**, *92*, 69.

Insulin-loaded albumin-conjugated porous silicon nanoparticles encapsulated into pH-sensitive polymer. The formulation shows tunable size and size distribution, morphology, high cytocompatibility, and controlled drug release profile. Insulin permeation across the intestinal epithelium is higher when loaded into albumin-decorated nanoparticles. The nanoparticles hijack the FcRn transcytotic pathway, and cross the epithelial cell layer, improving insulin delivery.

Nanoparticles

J. P. Martins, R. D'Auria, D. Liu, F. Fontana, M. Ferreira, A. Correia, M. Kemell, E. Mäkilä, J. Salonen, L. Casettari, J. Hirvonen, B. Sarmento, and H. A. Santos*

Engineered Multifunctional Albumin-Decorated Porous Silicon Nanoparticles for FcRn Translocation of Insulin

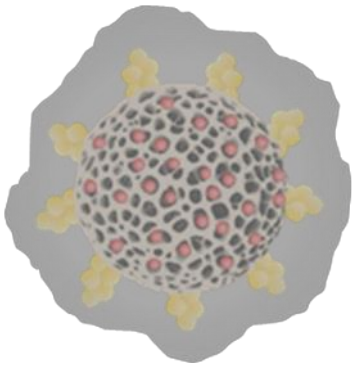

Copyright WILEY-VCH Verlag GmbH & Co. KGaA, 69469 Weinheim, Germany, 2016.

Supporting Information

Engineered Multifunctional Albumin-Decorated Porous Silicon Nanoparticles for FcRn Translocation of Insulin

João P. Martins, Roberto D'Auria, Dongfei Liu, Flavia Fontana, Mónica P. A. Ferreira, Alexandra Correia, Marianna Kemell, Karina Moslova, Ermei Mäkilä, Jarno Salonen, Luca Casettari, Jouni Hirvonen, Bruno Sarmento, and Hélder A. Santos**

J. P. Martins, R. D'Auria, Dr. D. Liu, F. Fontana, M. P. A. Ferreira, A. Correia, E. Mäkilä, Prof. J. Hirvonen, Prof. H. A. Santos
Drug Research Program, Division of Pharmaceutical Chemistry and Technology, Faculty of Pharmacy, University of Helsinki, Helsinki FI-00014, Finland
E-mail: joao.martins@helsinki.fi; helder.santos@helsinki.fi

R. D'Auria, Prof. L Casettari
Department of Biomolecular Sciences, School of Pharmacy, University of Urbino, Urbino (PU) 61029, Italy

Dr. D. Liu, Prof. H. A. Santos
Helsinki Institute of Life Science (HiLIFE), University of Helsinki, Helsinki FI-00014, Finland

Dr. M. Kemell
Department of Chemistry, University of Helsinki, Helsinki FI-00014, Finland

E. Mäkilä, Prof. J. Salonen
Laboratory of Industrial Physics, Department of Physics and Astronomy, University of Turku, Turku FI-20014, Finland

Prof. B. Sarmento
i3S - Instituto de Investigação e Inovação em Saúde, University of Porto, 4200-135 Porto, Portugal

Prof. B. Sarmento
INEB - Instituto de Engenharia Biomédica, University of Porto, 4200-135 Porto, Portugal

Prof. B. Sarmento
CESPU - Instituto de Investigação e Formação Avançada em Ciências e Tecnologias da Saúde, 4585-116 Gandra, Portugal

Keywords: albumin; FcRn; insulin; nanoparticles; oral delivery

1. Experimental Section

Materials: ChromPure Human Albumin and Alexa Fluor® 488-ChromPure Human IgG, Fc fragment were purchased from Jackson ImmunoResearch Laboratories, Inc. (West Baltimore Pike, West Grove, PA, USA). Hypromellose acetate succinate (H grade fine powders; HPMC) was purchased from Shin-Etsu Chemicam Co., Japan. CellMask™ DeepRed, Hank's Balanced Salt Solution (10× HBSS), fetal bovine serum (FBS), and Dulbecco's Modified Eagle Medium (DMEM) were purchased from Life Technologies Gibco®, USA. CellTiter-Glo® reagent assay was purchased from Promega Corporation, USA. Polycarbonate Transwell™ filters (3 μm pore size, 6- and 12-well plate) and 75 cm^2 cell culture flasks were purchased from Corning® Inc. (NY, USA). Human recombinant Insulin (MW 5800 Da), 2-(*N*-morpholino-ethanesulfonic acid (MES), 1-ethyl-3-(3-dimethylaminopropyl)-carbodiimide (EDC), N-hydroxysuccinimide (NHS), 2-(4-(2-hydroxyethyl)pipezarin-1-yl) ethanesulfonic acid (HEPES), bovine serum albumin (BSA), Ethyl acetate and Poly (vinyl alcohol) (PVA) were purchased from Sigma-Aldrich® (St. Louis, MO, USA). ZO-1 antibody Alexa Fluor® 594 conjugated, occludin antibody Alexa Fluor® 594 conjugated, and Versene solution were purchased from ThermoFisher Scientific (Waltham, MA, USA). Phosphate Buffered Saline (10× PBS), non-essential aminoacids (NEEA), L-glutamine 200mM, penicillin (100 IU mL^{-1}), streptomycin (100 mg mL^{-1}) and trypsin 2.5% were purchased from HyClone™, GE Healthcare Lifesciences (Logan, UT, USA). Vectashield® antifade mounting medium containing 2-(4-amidinophenyl)-1H -indole-6-carboxamidine (DAPI) was purchased from Vector Laboratories, Inc. (Burlingame, CA, USA). Triton X-100 was purchased from Merck Millipore (Darmstadt, Germany). Accutase® was purchased from Innovative Cell Technologies, Inc. (San Diego, CA, USA). All materials were used as received.

Preparation of undecylenic acid modified thermally hydrocarbonized porous silicon (UnPSi) nanoparticles: UnPSi NP were prepared by electrochemical anodization, as previously

reported.[1, 2] Briefly, free-standing PSi films were produced by electrochemical anodization of monocrystalline, boron-doped p+-type Si <100> wafers with a resistivity of 0.01–0.02 Ω/cm in a 1:1 (v/v) hydrofluoric acid (38%)–ethanol electrolyte. A repeated pulsed low/high etching profile, designed to create fracture planes on the Si wafers at desired intervals was used to form a multilayer structure. The multilayer film was then detached from the substrate by abruptly increasing the etching current to the electropolishing region. To remove residual moisture and oxygen, the fresh PSi multilayer films were exposed to N_2 flow (1 mL min^{-1}) for at least 30 min. The free standing multilayer PSi films were then thermally hydrocarbonized with acetylene (C_2H_2, 1 L min^{-1}), added to a 1 L min^{-1} N_2 for 15 min at room temperature (RT) and heat treated for 15 min at 500 ºC under the 1:1 (vol.) N_2/C_2H_2 flow. The thermally hydrocarbonized films were allowed to cool back to RT under N_2 flow. Afterwards, the films were immersed into undecylenic acid for 16 h at 120 ºC, in order to obtain undecylenic acid modified thermally hydrocarbonized porous silicon (UnPSi) films with –COOH termination. The UnPSi nanoparticles were obtained by wet milling using a high energy ball mill, and separated by centrifugation. The physical properties of the nanoparticles were evaluated by N_2 sorption isotherms (**Table S2**).

Immunostaining of tight junctions: C2BBe1/HT29-MTX were cocultured in 12-well Transwell™ filter membranes (3 μm pore-size; Corning Inc., USA) at a ratio of 90:10, respectively, and using a cell density of 68 × 10^4 cells per cm^2, with cell culture medium replaced every other day. C2BBe1 monocultures were used as control, following the same procedure described for the coculture. After 21 days in culture, C2BBe1 and C2BBe1/HT29-MTX monolayers were fixed in 4% PFA for 15 min. For the staining of zonula occludens-1 (ZO-1), cells were permeabilized with 0.05% Triton X-100 in 0.1 M PBS for 10 min at RT. After washings, non-specific binding was blocked with 10% BSA for 30 min, and then incubated with ZO-1 antibody (1:100) in 0.1 M PBS for 60 min at RT. For the staining of

occludin, non-specific protein interactions were blocked with 5% BSA for 5 min, and cells were incubated with occludin antibody (1:100) for 60 min at RT. After incubation with the antibodies, cells were extensively washed and Transwell™ filter membranes were cut and assembled with Vectashield® antifade mounting medium containing DAPI for nuclei counterstaining, and observed at Leica DM6000 B microscope (Leica Microsystems, Wetzlar, Germany).

Transepithelial electrical resistance (TEER) measurements: TEER values were measured using a Millicell® ERS-2 volt-ohm-meter with STX01 electrodes (Millipore, MA, USA). TEER values were calculated by subtracting the TEER of the blank Transwell™ filters (without cells) to the TEER presented by each Transwell™ with C2BBe1 or C2BBe1/HT29-MTX monolayers. This value was then multiplied by the surface area of the insert, and reported as $\Omega.cm^2$.

2. Results and discussion

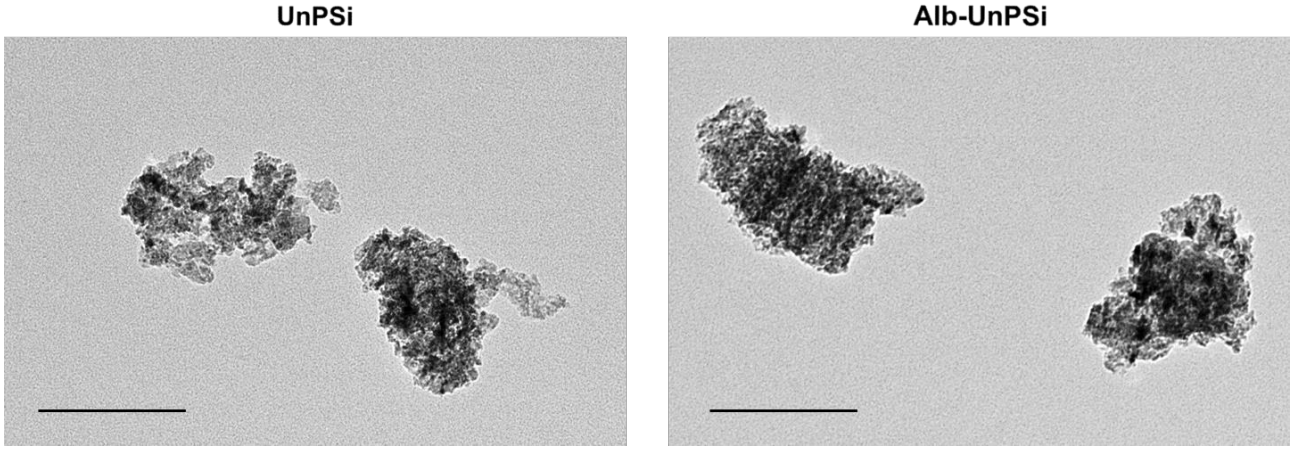

Figure S1. Representative TEM image of UnPSi and Alb-UnPSi NPs. Scale bar is 200 μm.

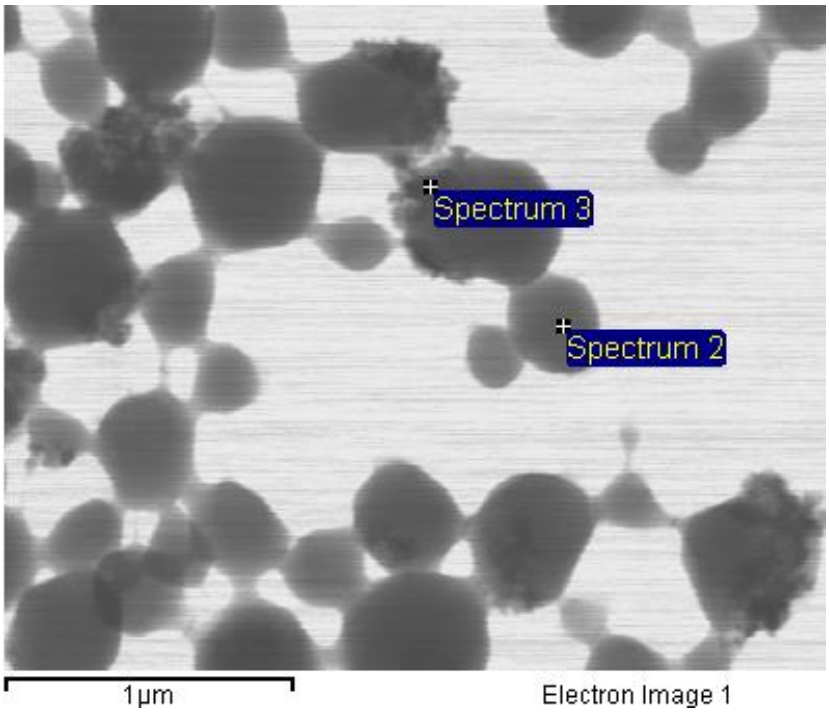

Figure S2. Representative TE image of Alb-UnPSi@HPMC NPs for analysis of the elemental composition by EDX, with Spectrum 2 corresponding to a bare HPMC particle, and Spectrum 3 corresponding to Alb-UnPSi@HPMC NPs, where Si is observed. Scale bar is 1 µm.

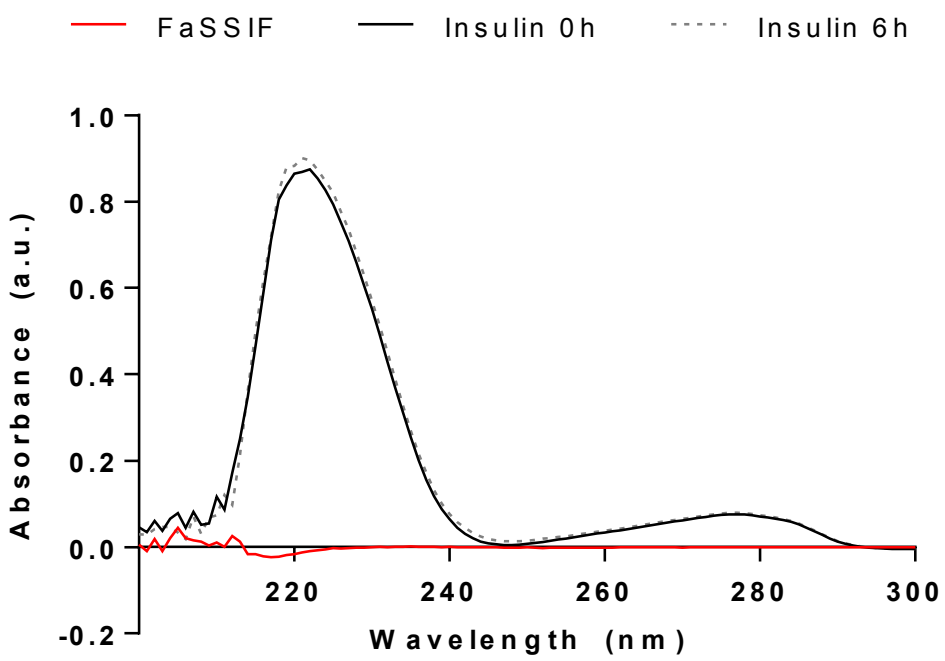

Figure S3. UV-Vis spectra of insulin in FaSSIF after preparation and after 6h incubation. Spectra of FaSSIF was used as control.

Immunostaining of tight junctions

The expression of tight junctions is essential for the proper functioning of the epithelial cells as a monolayer. C2BBe1/HT29-MTX were stained for zonula occludens (ZO)-1 and occludin. The expression of these tight junctions in C2BBe1 monoculture conditions was assessed as control. The presence of continuous and organized tight junctional molecules as ZO-1 and occludin was observed in the inter-epithelial cell contact of the cocultures as in the monoculture conditions (**Figure S4**).

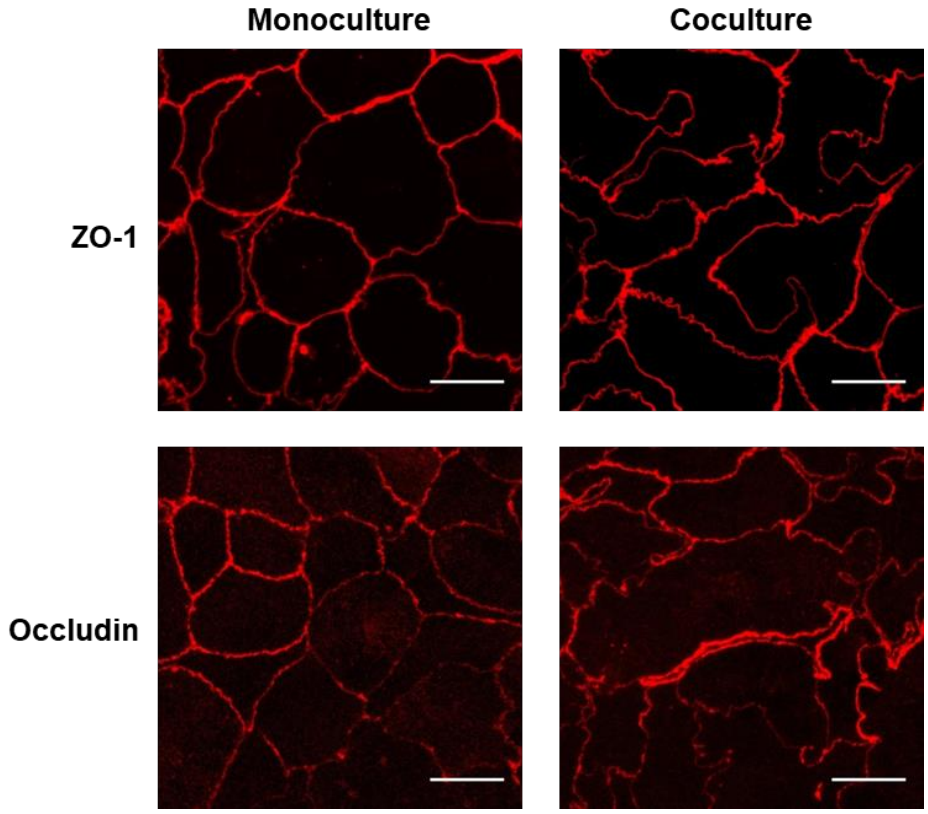

Figure S4. Junction proteins expressed by C2BBe1 when cultured alone (left panel) or cocultured with HT29-MTX (right panel). Confocal microscopy images show fixed and permeabilized C2BBe1 and C2BBe1/HT29-MTX cells grown on Transwell™ filters for 21 days, and stained with antibodies for ZO-1 (upper pannel) and occludin (lower pannel). Scale bar is 10 μm.

Monitoring of the TEER values

The successful establishment of tight junctions was further supported by the high TEER values obtained at the end of the culture period on *in vitro* C2BBe1 and C2BBe1/HT29-MTX monolayers. Results suggest that the epithelial cells were fully differentiated in what concerns the establishment of continuous tight junctions (**Figure S5**), and therefore ensuring the functionality of the model. TEER values for the cocultures were lower than those observed in the monoculture, which are translated in a more permeable membrane. This effect can be attributed to the presence of the HT29-MTX cells and, as already mentioned, resembles more accurately the *in vivo* microenvironment.

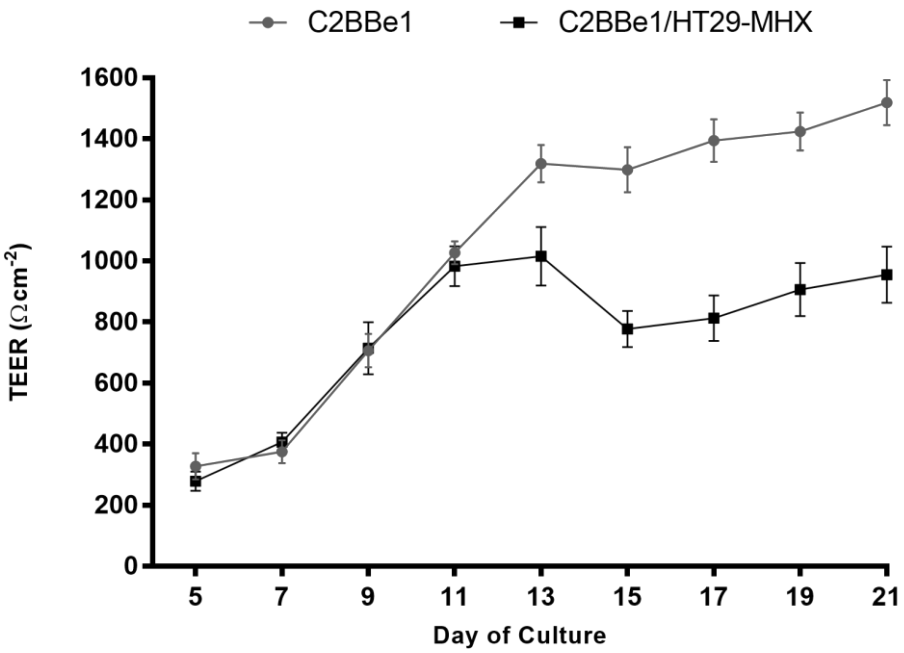

Figure S5. TEER values monitored from day 5 to 21 on *in vitro* C2BBe1 and C2BBe1/HT29-MTX monolayers grown in Transwell™ filters.

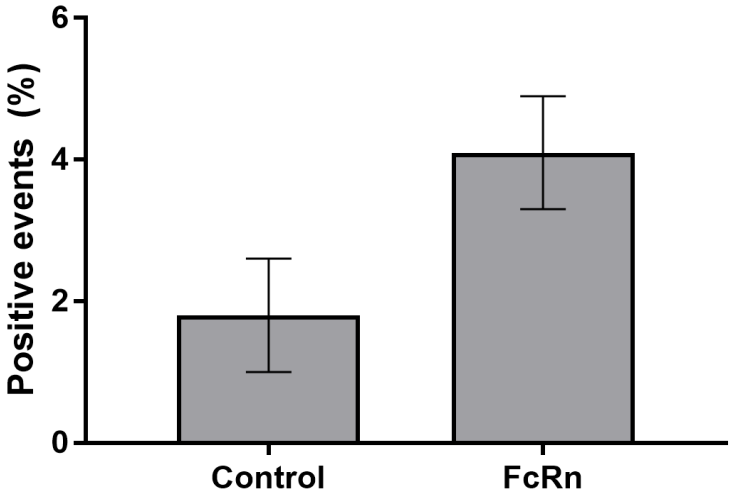

Figure S6. Flow cytometry quantitative analysis of C2BBe1/HT29-MTX coculture cells expressing FcRn after incubation with Alexa Fluor® 488 Fc fragment conjugated (3.96 μg mL^{-1}) for 3h at 37 °C in humidified atmosphere. Cocultures non-treated with Fc fragment were used as control.

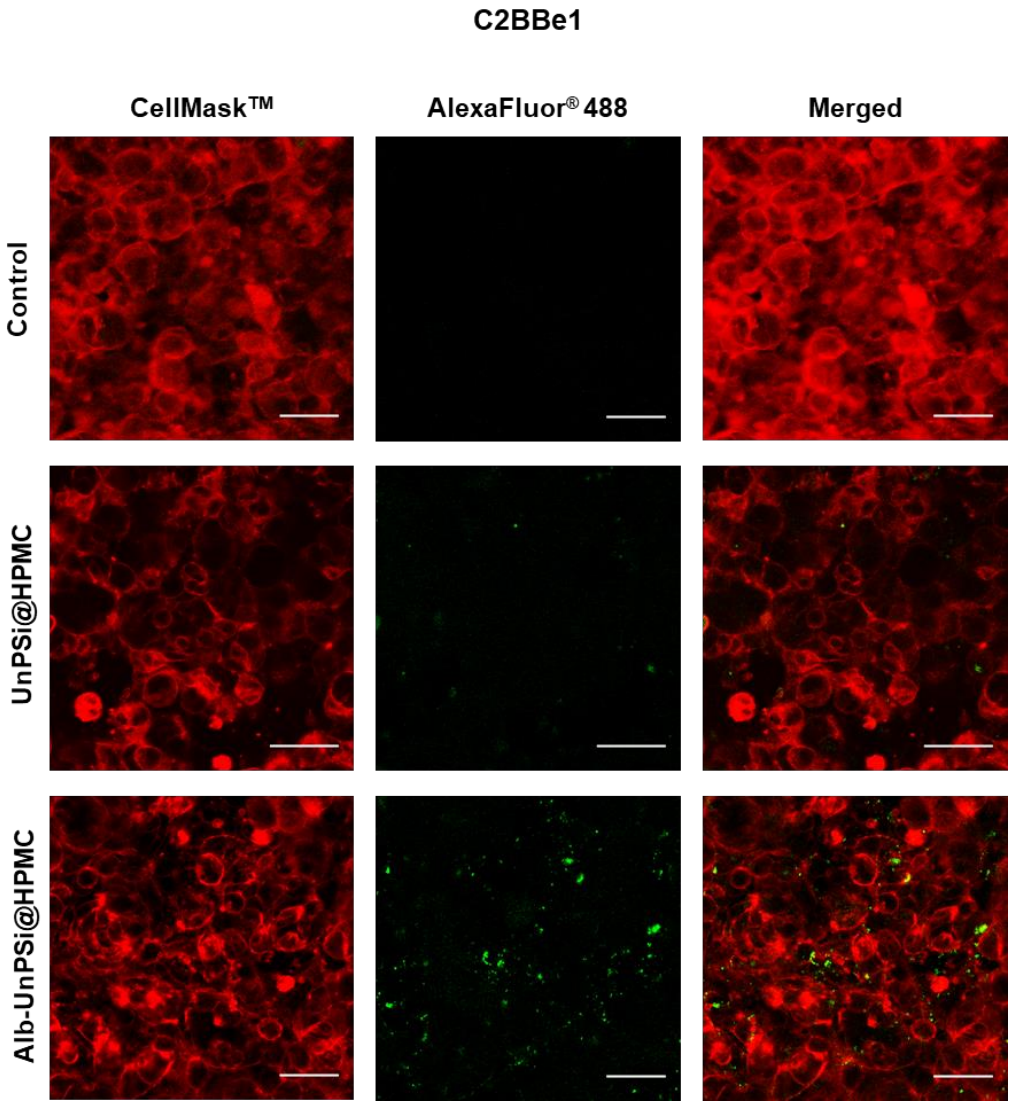

Figure S7. Interaction of the NPs with intestinal cells. Confocal microscopy imaging of C2BBe1 monocultures incubated with UnPSi@HPMC functionalized and non-functionalized with albumin for 3 h at 37 °C. Cell membranes were stained with CellMask™ Deep Red (red) and the different NPs were labeled with Alexa Fluor® 488 (green).

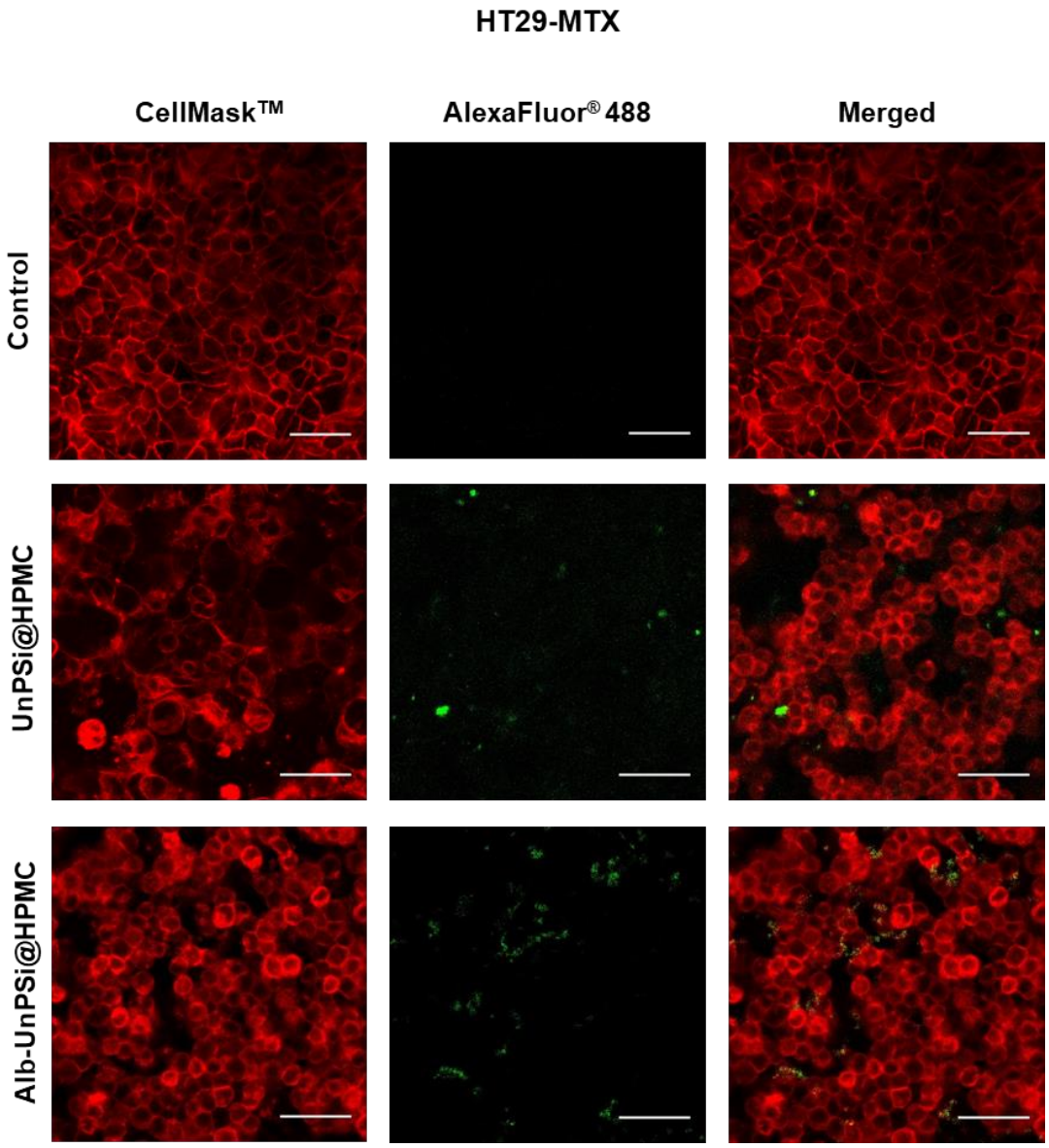

Figure S8. Interaction of the NPs with intestinal cells. Confocal microscopy imaging of HT29-MTX monocultures incubated with UnPSi@HPMC functionalized and non-functionalized with albumin for 3 h at 37 °C. Cell membranes were stained with CellMask™ Deep Red (red) and different NPs were labeled with Alexa Fluor® 488 (green).

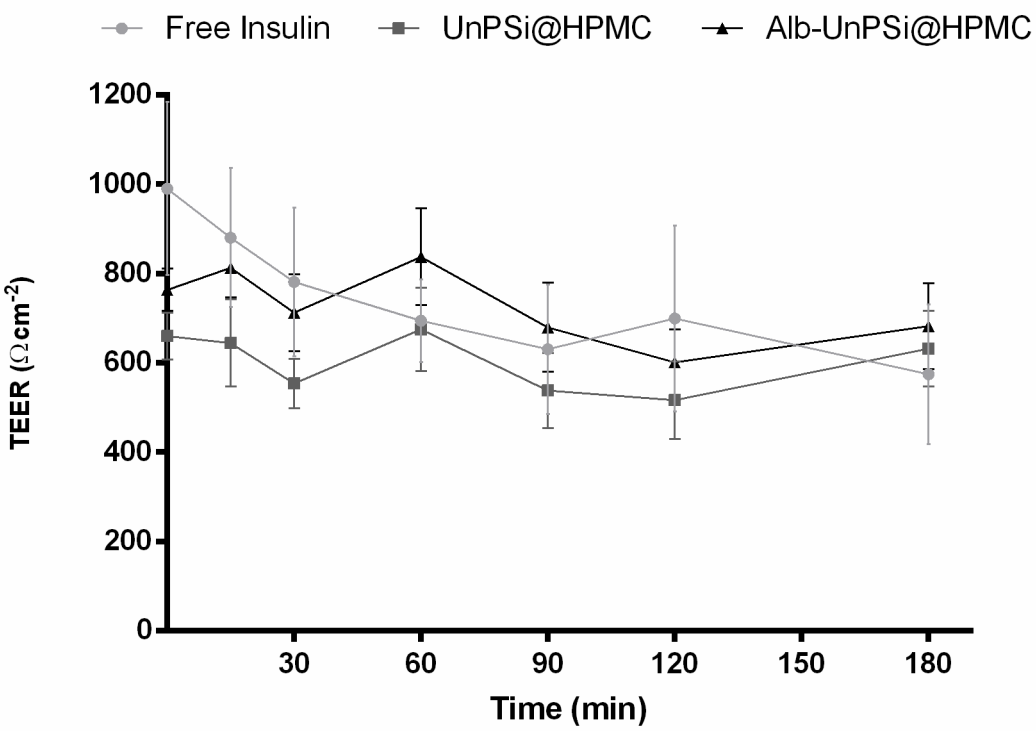

Figure S9. TEER values monitored during *in vitro* permeability test C2BBe1/HT29-MTX monolayers grown in Transwell™ filters at different time points for 3 h.

Table S1. Mass percentage of the elements N, C, H and S determined in the UnPSi and Alb-UnPSi NPs quantified by elemental analysis

Sample	N, %	C, %	H, %	S, %
UnPSi	-	14.03 ± 2.40	1.84 ± 0.09	–
Alb- UnPSi	1.80 ± 0.08	19.29 ± 1.40	2.81 ± 0.50	–

Table S2. N_2 sorption isotherms for surface area, total pore volume and pore diameter of UnPSi NPs.

Parameter	Value
Specific surface area	280 ± 5 m^2 g^{-1}
Total pore volume	0.60 ± 0.02 cm^3 g^{-1}
Average pore diameter	8.5 ± 0.1 nm

References

[1] N. Shrestha, M. A. Shahbazi, F. Araujo, E. Mäkilä, J. Raula, E. I. Kauppinen, J. Salonen, B. Sarmento, J. Hirvonen, H. A. Santos, *Biomaterials* **2015**, *68*, 9.
[2] M.-A. Shahbazi, N. Shrestha, E. Mäkilä, F. Araújo, A. Correia, T. Ramos, B. Sarmento, J. Salonen, J. Hirvonen, H. A. Santos, *Nano Res.* **2015**, *8*, 1505.

Scheme 1

Click here to access/download
Production Data
1 Scheme.tif

Figure 1

Click here to access/download

Production Data

Figure 1.tif

Figure 2

Figure 3

Click here to access/download

Production Data

Figure 3.tif

Figure 4

Figure 5

Figure 6

Figure 7

Graphical Abstract